Recombinant αβ-tubulin and a simple computational model shed light on the molecular mechanisms of microtubule dynamics

APPROVED BY SUPERVISORY COMMITTEE

Luke M. Rice, Ph.D.

Rama Ranganathan, Ph.D.

Elliott Ross, Ph.D.

Hongtao Yu, Ph.D.

Acknowledgements

‘It was the best of times, it was the worst of times, it was the age of wisdom, it was the age of foolishness, it was the epoch of belief, it was the epoch of incredulity, it was the season of Light, it was the season of Darkness, it was the spring of hope, it was the winter of despair, we had everything before us, we had nothing before us.’

- Charles Dickens, *A Tale of Two Cities*

The above sums up graduate school for me. And I don’t damn the ambiguity, but celebrate it. The last few years have been fun and stressful. I thank Luke for teaching me ‘how to get shit done’, and I thank my labmates both past and present for their trust and friendship. A little lady and labmate from Delhi advised me to give special thanks to the ‘extraordinarily brilliant, charming and fearless women in my life. ;)’ I’m ready to try the wings I’ve gained over 5 years of exertion and hope they don’t fail me too soon. I give supreme thanks to my family (my beautiful habibi, my adorable mother, my model father, my rediscovered brother and adoring sister). Without the love I receive daily from Ilse, my wife of 2 years, and my parents, I’d be as withered and uninspired as an earthworm left on the concrete in the middle of a dry Texas summer. The three form some sort of Holy Trinity for me, a devout secular humanist. I also have many many friends and acquaintances to thank (truly, too numerous to mention) for the kind and inspiring things they’ve done for me (both wittingly and unwittingly) over the years. (A special shout-out to my thammudu Sai Medi, a friend of many years and a fellow vudumu who, like me, is in constant search of the transcendent).

RECOMBINANT AB-TUBULIN AND A SIMPLE COMPUTATIONAL MODEL SHED LIGHT ON THE MOLECULAR MECHANISMS OF MICROTUBULE DYNAMICS

by

FELIPE-ANDRÉS PIEDRA

DISSERTATION / THESIS

Presented to the Faculty of the Graduate School of Biomedical Sciences

The University of Texas Southwestern Medical Center at Dallas

In Partial Fulfillment of the Requirements

For the Degree of

DOCTOR OF PHILOSOPHY

The University of Texas Southwestern Medical Center at Dallas

Dallas, Texas

May 2015

RECOMBINANT AB-TUBULIN AND A SIMPLE COMPUTATIONAL MODEL SHED LIGHT ON THE MOLECULAR MECHANISMS OF MICROTUBULE DYNAMICS

Publication No. _____

Felipe-Andrés Piedra, Ph.D.

The University of Texas Southwestern Medical Center at Dallas, 2015

Supervising Professor: Luke M. Rice, Ph.D.

Table of Contents

Acknowledgements ii

Table of Contents vi

Prior Publications viii

List of Abbreviations ix

Abstract 10

CHAPTER ONE

Introduction: Microtubule Structure and Dynamics 12

The discovery of microtubules and tubulin 12

A brief note on cytoskeletal proteins in bacteria, archaea and viruses 15

MT structure 15

Figure 1. Three structures of GTP-bound αβ-tubulin adopt similar curved conformations. *Figure and legend taken from (Brouhard and Rice, 2014).* 19

MT dynamics 21

The effect of nucleotide-state on αβ-tubulin 22

Figure 2. Cis-acting vs. trans-acting nucleotide. 25

MT dynamics in vitro 26

Figure 3. A one-dimensional (1D) model offers insight into the biochemistry of MT elongation and shrinking. 28

MT dynamics in silico 31

CHAPTER TWO

Implications of Trans-acting GTP for Microtubule Catastrophe 35

Introduction 36

Methods 36

Figure 1. Rates of MT elongation depend on the on-rate constant (kon) and binding affinities. 41

Figure 2. The rate of MT shrinking depends on the corner affinity and the GDP-weakening effect. 44

Figure 3. The catastrophe frequency depends sensitively on concentration and the GTPase rate, and also depends on the rate of GDP to GTP exchange on the MT end 46

Results 51

Figure 4. A kinetic Monte Carlo model where the nucleotide acts in trans reproduces benchmark observations of porcine MT elongation and shrinking rates. 53

Figure 5. A potential role for GDP to GTP exchange in microtubule catastrophe is revealed by implementing trans-acting nucleotide into a Monte Carlo model of MT dynamics. 55

Figure 6. C12A yeast ab-tubulin binds less tightly to GDP, and C12A microtubules elongate comparably to wild-type but undergo catastrophe less frequently. 59

Figure 7. αβ-tubulin binds less tightly to 2'-deoxy GDP (dGDP) than to GDP, and polymerization in the presence of dGTP gives less frequent catastrophe than with GTP. 61

Figure 8. The C12S mutation suppresses catastrophe but also significantly affects rates of MT elongation. 63

Figure 9. Deoxyguanosine nucleotides bind less tightly to yeast αβ-tubulin. 64
Figure 10. Exploring the effect of altered GDP to GTP exchange rates on MT catastrophe 66
Discussion 68

CHAPTER THREE

Comparing Microtubule Dynamics from Divergent αβ-tubulins 69
Abstract 69
Introduction 70
Methods 71
Results 73
Figure 1. Yeast MTs polymerize and depolymerize more readily than porcine MTs. 76
Figure 2. A mixture of binding sites exists on the MT end. 78
Figure 3. Yeast microtubules (MTs) in vitro elongate from plus-ends exclusively. 79
Figure 4. Porcine MT elongation rates show temperature sensitivity from 30 to 37 °C 82
Figure 5. Our model captures both yeast and porcine MT dynamics data. 86
Figure 6. Our model captures the catastrophe frequency of yeast MTs at one concentration of αβ-tubulin 88
Discussion 89

CHAPTER FOUR

Conclusions and Future Directions 94
Implications of trans-acting GTP for MT catastrophe 94
Comparing MT dynamics from divergent αβ-tubulins 96
Future Directions 100
Microtubule dynamics in vitro 100
The model 103

Bibliography 108

Prior Publications

Ayaz P, Munyoki S, Geyer EA, **Piedra FA**, Vu ES, Bromberg R, Otwinowski Z, Grishin NV, Brautigam CA, Rice LM. (2014) "A tethered delivery mechanism explains the catalytic action of a microtubule polymerase." eLife 10.7554/eLife.03069.

List of Abbreviations

DICM – differential interference contrast microscopy

DRaCALA – differential radial capillary action of ligand assay

μM – micro molar

MT – microtubule

EM – electron microscopy

SDS-PAGE – sodium dodecyl sulfate polyacrylamide gel electrophoresis

SAXS – small angle x-ray scattering

nm – nanometer

μm – micron or micrometer

kon – on-rate constant ($\mu M^{-1}sec^{-1}$)

koff – off-rate constant (sec^{-1})

TIRFM – total internal reflection fluorescence microscopy

FRET – fluorescence-resonance energy transfer

ITC – isothermal calorimetry

AAA – amino acid analysis

AUC – analytical ultracentrifugation

Abstract

Microtubules (MTs) are essential to all eukaryotic organisms. They help segregate chromosomes and organize the cytoplasm. MTs are hollow barrels of the protein αβ-tubulin that exhibit a non-equilibrium behavior called dynamic instability: the stochastic switching of single polymers from a state of gradual growth to one of rapid disassembly. Dynamic instability underlies the MT cytoskeleton's rapid reorganizability and enables its diversity of functions. MTs can be reconstituted from purified αβ-tubulin and have been studied in vitro for over 40 years. Over this time, huge strides have been made in the development of an understanding of dynamic instability. Nevertheless, the mechanistic basis of important phenomena like GTP-dependent assembly and GTP hydrolysis-induced conformational change and catastrophe (the switch from growing to shrinking) remain controversial or unexplained. In Chapter 2, I discuss a study in which we used a computational model to investigate the consequences of a new way of thinking about the effect of nucleotide-state on αβ-tubulin and MT assembly. Our results suggest that GDP exposure on the MT plus-end can frustrate elongation and lead to catastrophe. We therefore predicted that GDP to GTP exchange on the MT plus-end might reduce the frequency of catastrophe. We tested our prediction by analyzing the effects of a mutant αβ-tubulin and a GTP analog designed to increase the rate of terminal nucleotide exchange on MT dynamics in vitro. Our experimental results support the results from our model. Thus, we believe that GDP exposure on the MT plus-end increases the likelihood of catastrophe, and can be countered by GDP to GTP

exchange. In Chapter 3, I discuss a comparison of yeast and porcine MT dynamics in vitro. My measurements reveal striking differences between yeast and mammalian MT dynamics, and provide new constraints for models of MT dynamics. I conclude my thesis in Chapter 4 with my view of what my work means, what remains to be done and what paths my work has opened for further exploration.

CHAPTER ONE

Introduction: Microtubule Structure and Dynamics

The discovery of microtubules and tubulin

The German anatomist Walther Flemming observed microtubules in fixed and stained cells more than one hundred and thirty years ago (Flemming, 1965) (see (Paweletz, 2001) for a review of his life and work). Specifically, he was the first to observe the mitotic spindle (from the Greek word *mitos* meaning *thread*) and named it such after the thready appearance of the brightly stained chromosomes and the more dimly stained spindle fibers; however, many at the time believed the spindle fibers were artifactual because they were faint and could not be consistently observed. It would be another seventy years before the world was convinced that spindle fibers were biologically real and another decade or so after that before it was realized that they were microtubules (Inoue, 1953; Inoue, 1981; Inoue and Salmon, 1995).

Katsuma Dan and Shinya Inoue were responsible for proving the existence of spindle fibers (Okada, 1996; Dell and Vale, 2004; Inoue, 2008). Dan and Inoue were a teacher-student duo at the Musashi High School in Tokyo when, during the height of World War II and under constant air raids, they decided to attempt to visualize the mitotic spindle in living cells. Motivating Dan was a deeply held conviction that direct visualization of living processes was essential for the discovery of biological mechanism (Okada, 1996). Inspired by his teacher, Inoue set out to develop a microscope that would enable direct observations of the mitotic

spindle, and rapidly built a polarized light microscope out of the end of a discarded machine gun, a tin can, some string, and the appropriate optics (Burris and Segal, 1994; Dell and Vale, 2004; Inoue, 2008). A short time later, Inoue made the first ever observations of a 'living' mitotic spindle (Inoue, 1951; Inoue, 1953): Inoue saw dynamic fibers and fibrils-- he could watch them grow, fluctuate in length, and disappear. And when he lowered the temperature, they disappeared all at once; and when he brought it back up, they reappeared, and so on for arbitrarily many cycles. Inoue observed the same effect from the successive application and dilution of the drug colchicine, a known mitosis inhibitor (Inoue, 1981; Inoue and Salmon, 1995). Inoue deduced from these observations that spindle fibers and fibrils consisted of 'a loosely coupled, linear chain of protein molecules . . . in a temperature-sensitive dynamic equilibrium with their pool of subunits . . . The assembly was entropy driven, and the equilibrium toward polymer formation was favored at elevated temperatures and less favored at a lower temperature' (Inoue, 1951; Inoue, 1959). This was an illuminating and seminal conclusion: scientists, my advisor and myself included, are still trying to understand the basic mechanisms of spindle fibril (microtubule) dynamics; also, how the mitotic spindle, its myriad associated proteins, and chromatin interact to segregate chromosomes with high fidelity during cell division remains a fundamental mystery.

The protein composing spindle fibrils would stay unknown for close to two decades. In the early 1960s, improved fixatives enabled the first clear observations of spindle fibrils and other filaments in a variety of cell types by electron microscopy (EM); those studies revealed the same hollow, tube-like shape, suggesting that the imaged structures were fundamentally

the same and leading to the name microtubules (Wells, 2005b; Inoue, 2008). At around the same time, a biophysicist at the University of Chicago named Edwin Taylor became interested in the mechanism of action of colchicine. Gary Borisy, Taylor's graduate student, used radioactive colchicine to show binding activity in numerous cell and tissue types; initially worried by its apparent promiscuity, Borisy soon realized that the binding activity of colchicine correlated with the presence of microtubules (Wells, 2005a; Borisy and Taylor, 1967a; Borisy and Taylor, 1967b). Borisy then showed by zone sedimentation through a sucrose density gradient that radioactive colchicine exposed to a variety of cell extracts migrated consistently as a single peak, suggesting a single type of colchicine-macromolecule complex. From these and other data, Borisy and Taylor proposed that the bound molecule was the protein subunit of microtubules (Borisy and Taylor, 1967a; Borisy and Taylor, 1967b). A year later the protein would be sequenced by Hideo Mohri of the University of Tokyo, and given the name that Borisy and Taylor found 'jarring', tubulin (Mohri, 1968; Wells, 2005a). It would take another former graduate student of Edwin Taylor's, Richard Weisenberg, to finally prove that tubulin was the subunit of microtubules (Weisenberg, 1972; Inoue, 2008). Weisenberg tested the effects of different buffers on microtubule polymerization in crude cell extract and showed that a single component, Ca^{2+}, had thwarted all previous attempts to assemble microtubules from partially purified tubulin (Weisenberg, 1972). Tubulin could now be purified and repolymerized into structures that were identical to microtubules in fixed and stained cells.

Today we know much more about microtubule and tubulin structure, and the mechanisms by which αβ-tubulin gives rise to microtubule dynamics; nevertheless, fundamental mysteries remain. The remainder of the introduction should convey our current understanding and mention some important unknowns.

A brief note on cytoskeletal proteins in bacteria, archaea and viruses

Only recently has it become appreciated that bacteria and archaea abound in cytoskeletal proteins, among them tubulin and actin homologues (Graumann, 2007; Ettema et al., 2011; Wickstead and Gull, 2011; Shih and Rothfield, 2006). Like their eukaryotic counterparts, these proteins segregate DNA and contribute to cell morphogenesis and division. Additionally, both tubulin and actin homologues are involved in the segregation and stable inheritance of low-copy-number plasmids (Aylett and Lowe, 2012; Polka et al., 2009; Garner et al., 2007); and some of these plasmid-partitioning systems are even encoded by phages (Oliva et al., 2012; Kraemer et al., 2012). The ubiquity of tubulin and other cytoskeletal proteins indicates that polymerizing proteins are ancient and fulfill a critical function in cells, one that involves bridging otherwise separate spatiotemporal scales.

MT structure

Microtubules are hollow barrels of αβ-tubulin. They are ~25 nm in diameter and consist of laterally associated linear strands, or protofilaments, that run parallel to the major axis of the microtubule body. Microtubules tend to consist of 13 protofilaments *in vivo* (Desai and

Mitchison, 1997). Protofilament number can vary as a function of the nucleating structure and the β-tubulin isoform (more about αβ-tubulin to come) (Desai and Mitchison, 1997; Raff et al., 1997; Pucciarelli et al., 2012). Regulatory proteins can also affect protofilament number (Choi et al., 2009; Bechstedt and Brouhard, 2012) and it even varies *in vitro* as a function of the guanine nucleotide-- for example, GMPCPP predominantly gives rise to 14 protofilament MTs (Hyman et al., 1995). The functional consequences of different protofilament numbers are for the most part unknown. It is not known why, say, microtubules in the dendrites and axons of developing neurons consist solely of 13 protofilaments (Conde and Caceres, 2009; Bechstedt and Brouhard, 2012).

Each protofilament is comprised of αβ-tubulin subunits associated head to tail, where αβ-tubulin is an obligate heterodimer of α- and β-tubulin monomers, each with a molecular mass of ~50,000 daltons. αβ-tubulin is highly conserved across eukaryotic species with a sequence identity of ~70% (Neff et al., 1983; Schatz et al., 1986); and within species, the α- and β-monomers have a sequence identity of ~50% (Burns, 1991; Desai and Mitchison, 1997). The α- and β- monomers are structurally different, and because αβ-tubulin subunits associate head to tail, their polarity gives rise to a polarity in the microtubule body. The MT end where β-tubulin is exposed is the plus-end; and the end where α-tubulin is exposed is the minus-end. The plus-end of the microtubule is much more dynamic than the minus-end *in vivo*: it probes cytoplasmic space and acts as substrate for many regulatory proteins, while the minus-end is typically static and bound to some nucleating structure (Desai and Mitchison, 1997; Howard and Hyman, 2003). Going around the major axis of the microtubule, the lateral contacts

between αβ-tubulin subunits of neighboring protofilaments are homotypic: β-tubulin contacts β-tubulin and α-tubulin contacts α-tubulin-- except at the seam, a single longitudinal stretch where lateral contacts are heterotypic (Desai and Mitchison, 1997). The seam is a consequence of the microtubule's helicity and protofilament number-- where helicity refers to the 10° pitch in the lateral bonds of adjacent protofilaments, creating a helical path that winds around the MT lattice (Desai and Mitchison, 1997). Given a 10° pitch, a seam is inevitable so long as the protofilament number is 11 to 15 (Desai and Mitchison, 1997). The significance of the seam has been a mystery for decades (because it is not known to what degree the seam differs from the rest of the microtubule lattice energetically), but recent work by Katsuki et al. strongly suggests that the seam destabilizes the MT lattice (Katsuki et al., 2014).

Both α- and β-tubulin bind a single guanine nucleotide: α-tubulin binds exclusively to a non-exchangeable GTP buried at the interface of α- and β-tubulin, while β-tubulin binds a GTP or GDP that is solvent-exposed and exchangeable in unpolymerized αβ-tubulin and, less appreciated, at the plus-end of the microtubule (Mitchison, 1993; Caplow and Shanks, 1995).

A number of high-resolution structures of αβ-tubulin exist. The first was solved by cryo-electron crystallography on zinc-induced sheets of αβ-tubulin, revealing a compact protein with two highly similar monomers each consisting of a core of two beta-sheets wrapped in alpha helices (Nogales et al., 1998b). Later structures of αβ-tubulin were solved by x-ray crystallography and in complex with diverse regulatory proteins (Gigant et al., 2000; Ravelli

et al., 2004; Nawrotek et al., 2011; Pecqueur et al., 2012; Ayaz et al., 2012). A comparison of these structures reveals one major difference: curvature. Whereas the first structure is straight, all subsequent structures solved by x-ray crystallography are curved. The curvature of αβ-tubulin is reported in degrees, and refers to the size of the rotation needed to align the α- and β-subunits of a single αβ-tubulin structure. In the first structure, no rotation is needed-- only a translation, while in all subsequent structures β-tubulin has to be rotated by 10 to 13° for the two subunits to align optimally (Fig. 1) (Brouhard and Rice, 2014). The potential role/s of curvature in MT dynamics will be discussed further in the next section.

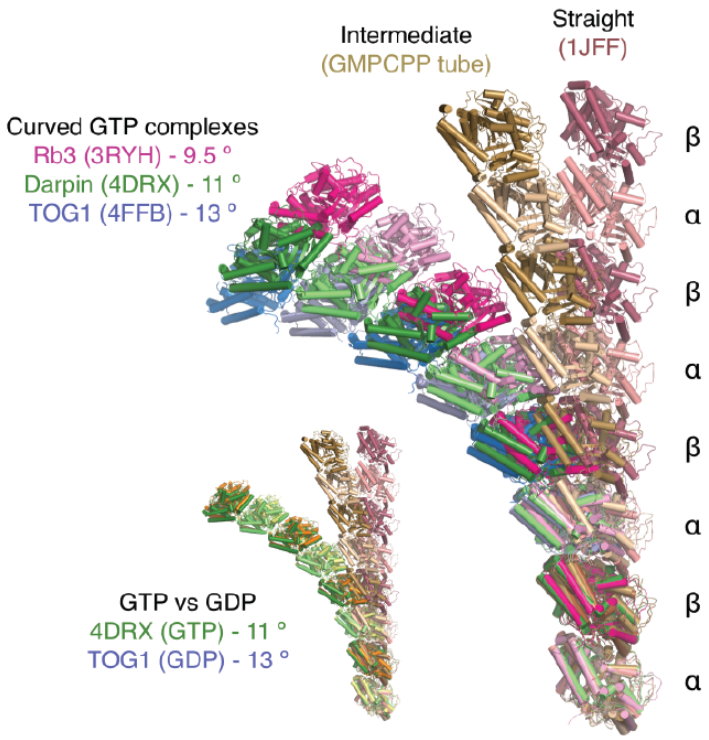

Figure 1. Three structures of GTP-bound αβ-tubulin adopt similar curved conformations. ***Figure and legend taken from (Brouhard and Rice, 2014).***

Different αβ-tubulin structures were superimposed using α-tubulin as a reference, and oligomers were generated by assuming that the spatial relationship between α- and β-tubulin within a heterodimer is identical to the relationship between heterodimers. Curvature is calculated from the rotational component of the transformation required to superimpose the α-tubulin chain onto the β-tubulin chain of the same heterodimer. All of the GTP-bound structures (Rb3 complex, Protein Data Bank [PDB] accession no. 3RYH [magenta]; DARPin complex, PDB accession no. 4DRX [green]; TOG1 complex, PDB accession no. 4FFB

[blue]) show between 10° and 13° of curvature, which is very similar to the curvature observed in GDP-bound structures (see inset, where the αβ-tubulins from a GDP-bound stathmin complex [PDB accession no. 1SA0] are shown in yellow and orange). A straight protofilament (putty and dark red color, PDB accession no. 1JFF) and a partially straightened assembly (tan) from GMPCPP ribbons are shown for reference.

MT dynamics

Single microtubules constantly switch between states of gradual growth and rapid disassembly: a property termed dynamic instability. Dynamic instability is essential. It underlies the rapid reorganizability of the MT cytoskeleton and enables its diversity of functions.

Tim Mitchison discovered dynamic instability as a graduate student in Marc Kirschner's lab in 1984 (Mitchison and Kirschner, 1984b; Mitchison and Kirschner, 1984a). At the time most MT dynamics experiments were done using a readout like turbidity to explore the bulk properties of assembling microtubules. These experiments were indispensable for establishing the basic facts of MT dynamics (GTP-dependent assembly, assembly-dependent GTP hydrolysis, etc. (Carlier and Pantaloni, 1978; Carlier and Pantaloni, 1981; Carlier, 1982)), but they could not say much about single microtubules. This is important because a number of models describing the behavior of single microtubules could fit observations of bulk behavior (Kirschner and Terrell Hill worked extensively on a treadmilling theory of MT dynamics (Hill and Kirschner, 1982; Mitchison, 2013)); but different models might predict different MT length distributions. Thus, length measurements of many single MTs could provide an additional constraint from which the right (or closer to right) model could be inferred. Mitchison's clever decision was to analyze single microtubules while they assembled by taking and fixing small aliquots from an assembly reaction every few minutes; he then visualized the MTs by EM and measured their lengths and number concentration (the

latter just by counting the number of MTs in the field of view). Mitchison did this at multiple concentrations and performed dilution experiments to measure rates of microtubule shrinking (Mitchison and Kirschner, 1984b; Mitchison and Kirschner, 1984a). In short, Mitchison observed that 1) MTs shrank much more rapidly than expected given the concentration-dependence of growth, and 2) MT number concentration decreased while MT length increased at and below steady-state (the αβ-tubulin concentration where microtubule assembly is exactly balanced by disassembly). This meant that MTs were either growing or rapidly shrinking, and monomers liberated from MT depolymerization were driving further growth of the remaining microtubules. This was clear and unexpected evidence that MT dynamics involved the 'coexistence of two phases, with the majority of microtubules growing slowly balanced by the minority shrinking rapidly.' (Mitchison and Kirschner, 1984a) Mitchison and Kirschner concluded with a GTP-cap model that is the foundation for our current understanding (Mitchison and Kirschner, 1984a). In it, a GTP cap stabilizes the growing microtubule until its loss from GTP hydrolysis drives the MT into another phase wherein it rapidly shrinks from the loss of GDP-bound subunits.

The effect of nucleotide-state on αβ-tubulin

αβ-tubulin must be bound to GTP in order to assemble into microtubules at physiological ranges of concentration and temperature. Catastrophe (the switch from growing to rapid shrinking) requires the assembly-dependent hydrolysis of GTP to GDP (Carlier et al., 1984; Desai and Mitchison, 1997; Nogales et al., 1998), although how GTP hydrolysis leads to catastrophe remains unknown.

There are two competing models for the effect of nucleotide-state on αβ-tubulin: 1) the allosteric model and 2) the lattice model (Fig. 2). The allosteric (or cis-acting) model proposes that the conformation of αβ-tubulin (and hence its polymerizability) is nucleotide-dependent-- with GTP inducing a straight conformation compatible with the microtubule lattice and GDP inducing a curved conformation that is not (Melki et al., 1989; Wang and Nogales, 2005; Nogales and Wang, 2006). The lattice (or trans-acting) model proposes that nucleotide-state determines the strength of the longitudinal interaction-- with GTP creating a higher affinity longitudinal binding interface for the minus-end of another subunit than GDP (Buey et al., 2006; Rice et al., 2008; Nawrotek et al., 2011). These models are not mutually exclusive a priori, but one is strongly supported by existing data while the other is not. Evidence for the cis-acting model is indirect and comes mostly from cryo-EM data showing growing microtubules with fairly straight ends and shrinking microtubules with highly curved ends (Mandelkow et al., 1991). These data led to the conclusion that nucleotide-dependent differences in αβ-tubulin conformation inside of the MT reflected nucleotide-dependent differences in αβ-tubulin conformation *outside* of the MT; but recent structures and biochemistry strongly support the trans-acting model (Buey et al., 2006; Rice et al., 2008; Nawrotek et al., 2011). First, later cryo-EM structures show that growing MTs also have curved ends (Chretien et al., 1995)-- these ends are not as curved as the ends of shrinking MTs, but they suggest that αβ-tubulin is not straight when it is being incorporated into the microtubule lattice. Furthermore, measurements of single subunit conformation by small-angle x-ray scattering (SAXS) reveal no differences in conformation between GTP-

and GDP-bound αβ-tubulin (Rice et al., 2008); and diverse regulatory proteins known by x-ray crystallography to bind the fully curved conformation of αβ-tubulin have equal affinities for GTP- and GDP-bound αβ-tubulin (Honnappa et al., 2003; Ayaz et al., 2012; Pecqueur et al., 2012), strongly suggesting that the two are conformationally indistinguishable outside of the MT lattice. Although a contribution of nucleotide-state to the conformation of free αβ-tubulin cannot be completely ruled out (it is possible that nucleotide-state slightly shifts the thermodynamic equilibrium of curved and straight conformations), there is no evidence to suggest that there is one. Much of my doctoral work has involved exploring the consequences of the trans-acting model in the context of a computational model.

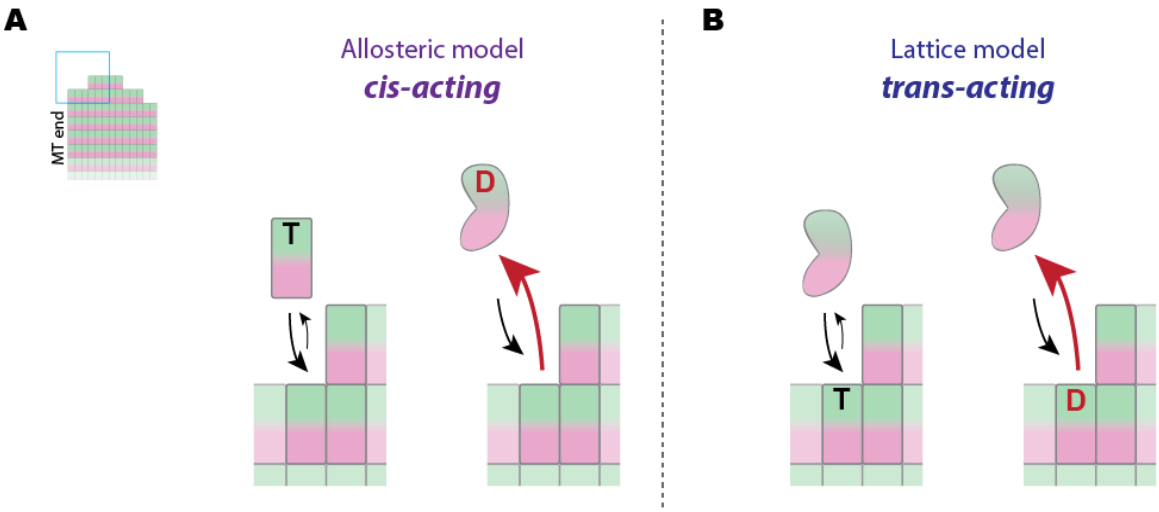

Figure 2. Cis-acting vs. trans-acting nucleotide.

Two competing models describe the effect of nucleotide-state on αβ-tubulin. (**A**) The allosteric (or cis-acting) model proposes that nucleotide-state acts in cis to determine the conformation and, hence, polymerizability of free αβ-tubulin (Melki et al., 1989; Wang and Nogales, 2005; Nogales and Wang, 2006). (**B**) The lattice (or trans-acting) model proposes that nucleotide-state acts in trans to alter the strength of longitudinal polymerization contacts, with GTP creating a binding interface of higher affinity than GDP. Furthermore, the trans-acting model proposes that free αβ-tubulin is curved independently of nucleotide-state, and that αβ-tubulin straightening occurs in the MT lattice. Existing data strongly support the trans-acting model (Buey et al., 2006; Rice et al., 2008; Nawrotek et al., 2011).

MT dynamics in vitro

Just two years after the foundational studies of Mitchison et al. (Mitchison and Kirschner, 1984b; Mitchison and Kirschner, 1984a), Tetsuya Horio and Hirokazu Hotani used dark-field microscopy to make the first real-time observations of single MTs at steady-state (Horio and Hotani, 1986), confirming that single MTs interconvert between states of gradual growth and rapid shrinking. Two years later, Walker et al. used video-enhanced differential interference contrast microscopy (VE-DICM) to record single MTs across a two-fold range of αβ-tubulin concentrations (Walker et al., 1988).

Walker et al. analyzed their recordings for four parameters of dynamic instability: 1) the rate of MT elongation; 2) the rate of MT shrinking; 3) the catastrophe frequency (the frequency of switching from growing to shrinking); and 4) the rescue frequency (the frequency of switching from shrinking to growing). They observed that the rate of MT elongation increased linearly with αβ-tubulin concentration while the rate of rapid MT shrinking was constant. They extracted biochemical information from their data using a one-dimensional (1D) model (Fig. 3). Their analysis suggested that the dissociation rate constant of GTP-bound αβ-tubulin from the growing MT lattice was much larger than previously estimated (Mitchison and Kirschner, 1984; Walker et al., 1988). They also observed that both catastrophe and rescue frequencies depended linearly, albeit softly, on concentration (the catastrophe frequency decreased and the rescue frequency increased with concentration). They surveyed existing GTP-cap models and concluded that none was capable of reproducing the observed dependence of the catastrophe frequency on the αβ-tubulin

concentration. Almost thirty years later, all existing biochemical models of MT dynamics, including our own, predict a catastrophe frequency that depends too steeply on concentration.

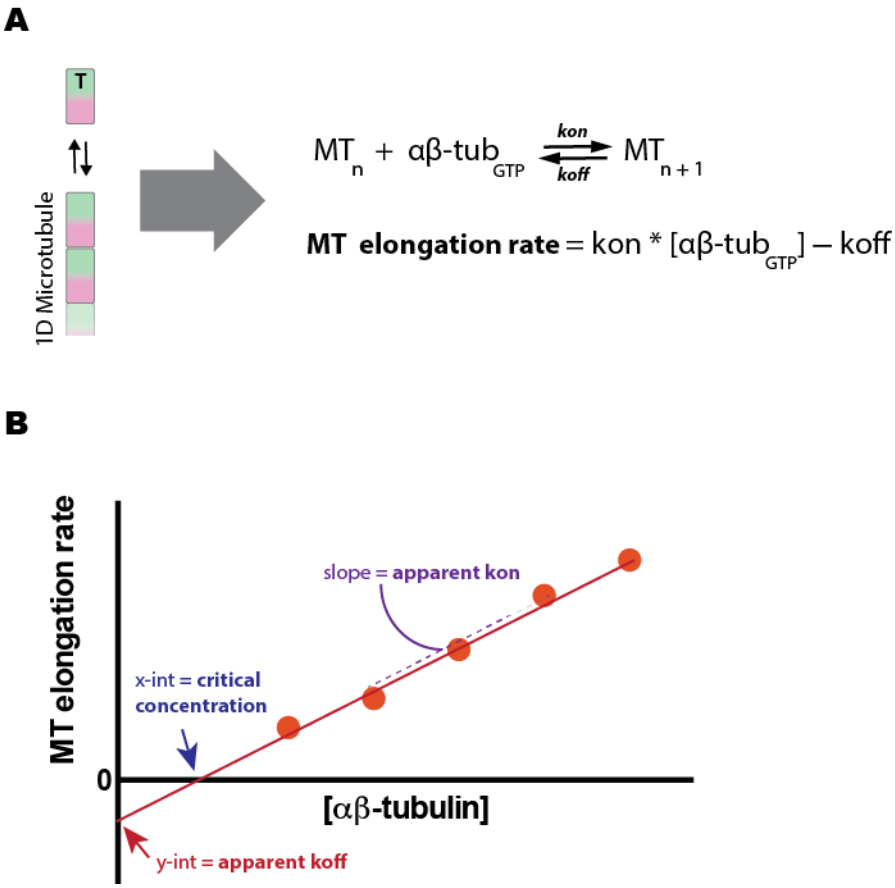

Figure 3. A one-dimensional (1D) model offers insight into the biochemistry of MT elongation and shrinking.

(**A**) A 1D model of a MT wherein subunit addition and dissociation occur to and from one site only predicts (right) that MT elongation results from a simple equilibrium between polymerized (MT) and free GTP-bound αβ-tubulin ($\alpha\beta\text{-tub}_{GTP}$). Where kon is the on-rate constant (units: $\mu M^{-1}s^{-1}$) defining the concentration-dependent arrival rate of GTP-bound αβ-tubulin onto the growing MT end; and koff is the off-rate constant (units: s^{-1}) defining the dissociation rate of $\alpha\beta\text{-tub}_{GTP}$ from the growing MT end. Consequently, the rate of MT elongation equals the kon * $[\alpha\beta\text{-tub}_{GTP}]$ (the concentration of $\alpha\beta\text{-tub}_{GTP}$) minus the koff. Using the same model, the rate of rapid, post-catastrophe shrinking equals the koff of GDP-bound αβ-tubulin ($\alpha\beta\text{-tub}_{GDP}$) from the MT end. (**B**) 'Apparent' biochemical rate constants can be derived by fitting the 1D model to observed rates of MT elongation and shrinking. An example plot of MT elongation rate vs. [αβ-tubulin]. The red points depict hypothetical data. Several biochemical parameters are retrievable from a line fit to the data: 1) the apparent on-rate constant (apparent kon) = slope; 2) the apparent off-rate constant (apparent koff) = y-intercept; and 3) the critical concentration (apparent koff/apparent kon) = x-intercept. The

term ‘apparent’ is used to make explicit the approximation made by fitting a one-dimensional model to data collected from real MTs; each apparent rate constant can be thought of as an average over multiple types of interactions present at the ends of real MTs.

Measurements of MT dynamics in vitro are now being made by total internal reflection fluorescence (TIRF) microscopy (Gardner et al., 2011b; Gardner et al., 2011a; Bechstedt and Brouhard, 2012; Zanic et al., 2013). TIRF microscopy permits the simultaneous imaging of labeled MTs and MT regulatory proteins, and therefore provides a greater opportunity to derive mechanism from imaging. Indeed, a number of TIRF-based studies have begun to elucidate the mechanisms of action of different MT regulatory proteins (Bechstedt and Brouhard, 2012; Zanic et al., 2013). However, although these studies have reinforced the idea that the state of the MT end is crucial to MT dynamics, in general they have not done much to improve our basic understanding. One recent study is an exception (Gardner et al., 2011b). Gardner et al. analyzed the cumulative distribution of catastrophe times from porcine MTs (Gardner et al., 2011b). They found that a gamma distribution with a shape parameter of three best fit their observations; where the shape parameter-- if integer-valued-- defines the number of exponentially distributed random variables that can explain the distribution. Each exponentially distributed random variable can be equated to a step in the process by which a MT undergoes catastrophe. Thus, the results of Gardner et al. suggest that catastrophe is a multi-step process (ergo MTs age), however we know not what the steps are.

To date, only mammalian MT dynamics have been thoroughly characterized in vitro (Walker et al., 1988; Gardner et al., 2011a; Gardner et al., 2011b). The αβ-tubulin used in those studies was purified from bovine or porcine brain. A variety of αβ-tubulin isotypes and post-translational modifications (PTMs) exist in mammalian brain (Redeker et al., 1993; Schwarz et al., 1998), creating a heterogeneity that complicates the analysis of MT dynamics in terms

of the underlying biochemistry of αβ-tubulin:αβ-tubulin interactions. Reliance on mammalian αβ-tubulin also precludes site-directed mutagenesis, preventing the study of potentially interesting mutants. Additionally, the particulars of mammalian MT dynamics represent just one kind of MT dynamics (MTs exist throughout Eukaryota). It is therefore important to determine the extent to which MT dynamics are conserved among αβ-tubulins from divergent organisms; such information might help elucidate the core mechanisms of MT dynamics.

MT dynamics in silico

Computational models of microtubule dynamics have been around for over thirty years (Chen and Hill, 1983; Chen and Hill, 1985; Goodson and Gregoretti, 2010; Bowne-Anderson et al., 2013). They involve one or more protofilaments, and can be more or less mechanistically explicit. Biochemical models where the dynamics of the simulated MT emerge from the collective properties of individual subunits are physically realistic and are valuable in that they can bridge the gap between our understanding of the properties of αβ-tubulin and the microtubule as a whole.

The first multi-protofilament biochemical model of MT dynamics was published one year after the discovery of dynamic instability (Chen and Hill, 1985). The model of Chen et al. assumes a thirteen-protofilament MT that grows by helical extension from addition of GTP-bound subunits to a total of five sites. Helical extension from five sites was assumed for computational tractability and from uncertainty at the time over the nature of subunit addition

to the growing MT lattice (later cryo-EM studies helped to solidify our understanding that MT growth occurs by subunit addition to any of the thirteen protofilaments at any given time-- not just helically (Chretien et al., 1995; Desai and Mitchison, 1997)). The model of Chen et al. includes a number of biochemical rate constants as parameters: 1) nucleotide state-dependent association and dissociation rate constants; 2) a rate constant for GTP hydrolysis (including neighbor effects); and 3) a rate constant for GDP to GTP exchange at the MT end (the vast majority of succeeding models do not include this reaction). Chen et al. performed Monte Carlo simulations at a number of αβ-tubulin concentrations to find parameter values that reproduced dynamic instability. Their model is powerful in that it is both simple and capable of reproducing dynamic instability. Its major drawbacks are that it assumes helical growth and cis-acting nucleotide.

Seventeen years later VanBuren et al. also used a biochemical model to reproduce dynamic instability and furthermore attempted to capture benchmark observations of MT dynamics made in 1988 by Walker et al. (VanBuren et al., 2002) Like Chen et al.'s 1985 model, nucleotide-state acts in cis in VanBuren et al.'s model; but in contrast, VanBuren et al.'s model does not assume helical growth (a subunit can add with equal probability to any of 13 protofilaments at any given time) and neither includes neighbor effects on the rate of assembly-dependent GTP hydrolysis nor a rate of GDP to GTP exchange at the MT end. VanBuren et al. also parameterized their model somewhat differently from Chen et al.: instead of independently specifying every biochemical rate constant, they chose to deal in free energies-- a choice that simplified their model because every possible interaction of a

subunit with the MT lattice is a result of some combination of only two binding modes (longitudinal and lateral). Their model has the following parameters: 1) separate free energies for longitudinal and lateral bonds; 2) one GTP hydrolysis rate constant for all subunits in the MT lattice (minus those at the end, for which it was realized after Chen et al.'s 1985 paper that GTP hydrolysis was not possible (Nogales et al., 1998b)); and 3) a 'kinking energy' defining the weaker lateral binding energy a GDP-bound subunit was presumed to have for the MT lattice. After assuming an intrinsic on-rate constant (kon) defining the rate of arrival of subunits onto the MT end, VanBuren et al. ran Monte Carlo simulations on a fixed microtubule seed to find lateral and longitudinal binding energies that reproduced observed, concentration-dependent rates of MT elongation. They also found the kinking energy that reproduced the observed concentration-independent rate of MT shrinking. VanBuren et al. combined their binding energies with a finite rate of GTP hydrolysis and a rule for simulating nucleotide-state dependent structure at the MT end to find a value of the GTP hydrolysis rate constant that would reproduce the observed frequency of catastrophe at one concentration of αβ-tubulin (= 10 μM). VanBuren et al.'s model captures the observed rates of MT elongation and rapid MT shrinking. It also captures the observed frequency of catastrophe at a single concentration of αβ-tubulin, but it fails to capture the observed concentration-dependence of the catastrophe frequency-- instead predicting one that is too steep. Additionally, their inclusion of a kinking energy for any single GDP-bound subunit presumes a cis-acting nucleotide, while existing structural and biochemical evidence point strongly to a nucleotide that acts in trans (Buey et al., 2006; Rice et al., 2008; Nawrotek et al., 2011). Finally, the rule

invoked by VanBuren et al. for simulating nucleotide-state dependent structure at the MT end is untestable.

All existing biochemical models fail to reproduce MT aging and the shallow dependence of the catastrophe frequency on the concentration of αβ-tubulin. Notably, the 'mechanochemical' model of VanBuren et al. from 2005 has been reported to capture both (VanBuren et al., 2005; Coombes et al., 2013). However, it has only been shown to give rise to a shallow concentration-dependence across a narrow range of αβ-tubulin concentrations (6 to 8 μM vs. 7 to 16 μM measured by Walker et al.) (Coombes et al., 2013). Additionally, nucleotide-state is assumed to act in cis in this model. We are convinced that a simple and testable model that is consistent with known αβ-tubulin structure and biochemistry can be developed that would, among other things ideally, capture both MT aging and the shallow concentration-dependence of the catastrophe frequency.

CHAPTER TWO

Implications of Trans-acting GTP for Microtubule Catastrophe

This work is to be published as:
Piedra FA, Vu ES, Burns A, Ye X, Rice LM. (expected 2015) "Implications of trans-acting GTP for microtubule catastrophe."

Abstract

Microtubules are dynamic polymers of αβ-tubulin that have essential roles in chromosome segregation and organizing the cytoplasm. Catastrophe – the switch from growing to shrinking – occurs when a microtubule loses its stabilizing GTP cap. Recent evidence indicates that the terminal nucleotide controls the strength of polymerization contacts (trans-acting GTP), but current models do not incorporate this information. We investigated the consequences of trans-acting GTP using a computational model, observing that GDP exposure on the microtubule end slows elongation and that faster GDP to GTP exchange on the microtubule plus end decreases the frequency of catastrophe. Using mutant αβ-tubulin or modified GTP, we show experimentally that a more readily exchangeable nucleotide leads to less frequent catastrophe. Our results suggest that transient exposure of GDP-capped protofilaments slows elongation by reducing the number of favorable binding sites on the microtubule end. This slowing can lead to catastrophe by allowing erosion of the GTP cap, and it can be countered by terminal nucleotide exchange.

Introduction

Microtubule (MT) polymerization dynamics are essential for proper assembly and positioning of the mitotic spindle and for organizing the cytoplasm (reviewed in (Desai and Mitchison, 1997; Howard and Hyman, 2003)). The dynamic behavior of MTs results from the assembly-dependent GTPase activity of the polymerizing αβ-tubulin subunits. Growing MTs are stabilized by a cap of GTP-bound αβ-tubulin subunits; loss of this cap triggers catastrophe, the switch from growing to rapid shrinking, by exposing the more labile GDP-lattice. The molecular details of how GTP stabilizes MTs, and how GTP hydrolysis and loss of the GTP cap lead to catastrophe, remain the subject of debate. GTP was previously thought to act in cis (Wang and Nogales, 2005; Nogales and Wang, 2006; Melki et al., 1989), such that the nucleotide state of a subunit at the end of a MT would dictate how tightly that subunit was bound. Current evidence favors trans-acting GTP (Rice et al., 2008; Buey et al., 2006; Nawrotek et al., 2011), such that the nucleotide *underneath* a terminal subunit would control how tightly that terminal subunit was bound. In the present study we sought to gain insight into the possible mechanistic consequences of trans-acting GTP.

Methods

Kinetic Modeling

We wrote a computer program to perform kinetic Monte Carlo simulations of MT dynamics, implementing an algorithm similar to one described previously (VanBuren et al., 2002). Part of our implementation has been described elsewhere (Ayaz et al., 2014). Briefly, the

microtubule lattice is represented by a two dimensional lattice with a staggered periodic boundary condition to mimic the cylindrical microtubule structure, and 5 layers of the lattice were designated as a 'seed' and considered to be permanently occupied. The program simulates MT dynamics one biochemical reaction (subunit addition or dissociation, GTP hydrolysis, or GDP to GTP exchange) at a time. Our parameterization assumes that the nucleotide (GTP or GDP) acts in trans to affect the strength of longitudinal contacts with GTP contacts stronger than GDP ones (Figure 1A); nearly all prior models have assumed cis-acting GTP (Bayley et al., 1989; VanBuren et al., 2002; VanBuren et al., 2005; Brun et al., 2009; Coombes et al., 2013) (but see (Margolin et al., 2012) for a notable exception). The rate of subunit addition into any available site is given by k_{on}*[αβ-tubulin]. Occupied sites (excepting the seed) can dissociate at a rate given by k_{on}*K_D where K_D is the affinity of interaction, which is determined by the neighbor state (number and type of lattice contacts) and obtained from longitudinal and corner affinities through thermodynamic coupling (Erickson and Pantaloni, 1981; VanBuren et al., 2002). GTP hydrolysis is modeled for all nonterminal subunits as a zero-order reaction with rate constant k_{GTPase}. We also include a rate of GDP to GTP exchange on the MT end. Because of the high concentration of GTP in our assays, we assume that GDP release is rate limiting for GDP to GTP exchange. Accordingly we model exchange on terminal subunits as a zero-order reaction with rate constant $k_{exchange}$. Simulations begin with only 13 possible events (associations onto the end of each protofilament). Execution times for each event are determined by sampling a random number x between 0 and 1, and then calculating the time as -(1/*rate*)*ln(x), where *rate* gives the appropriate rate constant. At each step the event with the shortest execution time is

implemented, the simulation time is advanced accordingly, and the list of possible events and their associated rates is updated to account for changes in subunit neighbor state. To obtain the length (in μm) of a simulated microtubule at a given time, we divide the number of subunits by 1625, the number of αβ-tubulin subunits in 1 μm of microtubule.

Parameter optimization

To recapitulate experimentally observed, concentration-dependent rates of MT elongation, and as described previously (Ayaz et al., 2014), we performed a manual grid search using 'GTP only' (negligible GTPase rate constant) simulations to obtain longitudinal and corner (longitudinal+lateral) affinities. We next searched for the 'GDP-weakening' factor that would yield the experimentally observed concentration-independent rate of rapid microtubule shrinking. Briefly, the affinities we obtained were used to simulate MT elongation to a length of 1 μm, after which the concentration of free αβ-tubulin was dropped to 0 μM, resulting in shrinking from the loss of GTP-bound subunits at the microtubule end; the fold-difference between this shrinking rate and the observed rate of rapid shrinking was the 'GDP-weakening' factor. Finally, we searched for a GTPase rate constant that would give the appropriate frequency of catastrophe. This procedure essentially followed the approach outlined in (VanBuren et al., 2002). But after observing a slight decrease in elongation rates with inclusion of a finite rate of GTP hydrolysis, we realized that our parameters required a slight retuning. Specifically, affinities had to be tightened and the GDP-weakening factor had to be increased to compensate for both the GTPase-induced slowdown in MT growth and a slowdown in the rate of rapid shrinking. We again performed a manual grid search (but this

time with the GTPase rate constant found previously) to obtain longitudinal and corner affinities that reproduced observed, concentration-dependent rates of MT elongation. To obtain an improved GDP-weakening factor, we performed dilution experiments where the GTPase rate constant already identified (*not* an arbitrarily high GTPase rate) was implemented simultaneously with dilution; the fold-difference between this shrinking rate and the observed shrinking rate was the factor by which we increased the GDP-weakening factor. The improved affinities and GDP-weakening factor were then used for another much more restricted scan of the GTPase rate constant (because the affinities and the GDP-weakening factor changed only modestly, the GTPase rate constant did not have to change much) to find a total parameter set that exactly reproduced the observed rates of MT elongation and shrinking, and the observed catastrophe frequency (the latter at one concentration of αβ-tubulin only).

Sensitivity analysis

It is important to establish how sensitive our model is to changes in parameter values. To that end, we fit our model to benchmark observations of porcine MT dynamics (Walker et al., 1988) and determined how our model's output (rates of MT elongation and shrinking, catastrophe frequencies) changed in response to varying parameter values.

We first analyzed the sensitivity of MT elongation rates from our model. Three parameters determine concentration-dependent rates of MT elongation: 1) the intrinsic on-rate constant (kon); 2) the longitudinal affinity; and 3) the lateral affinity. The lateral affinity is the weaker

of the two. Most incoming subunits bind to longitudinal or corner (1 longitudinal + 1 lateral) sites on the MT end; and, because the longitudinal affinity tends to be weak with respect to the concentration of αβ-tubulin, addition to corner sites dominates MT elongation. It is therefore important to establish how simulated rates of MT elongation vary with the assumed kon and corner and longitudinal affinities. We did this by varying each of the three preceding parameters independently and analyzing their effects on the concentration-dependence of MT elongation rates (Fig. 1). Changing the kon by a factor of 1.25 up-or-down increases or decreases the slope (apparent kon) of the MT elongation rate by the same factor (Fig. 1A). Changing the longitudinal affinity also mainly affects the slope of the MT elongation rate (Fig. 1C), but more modestly than kon: a factor of 2 increase or decrease changes the apparent kon by a factor of 1.3 up-or-down. In contrast, varying the corner affinity by a factor of 2 up-or-down primarily affects the x-intercept (critical concentration) and alters the apparent kon minimally (Fig. 1B).

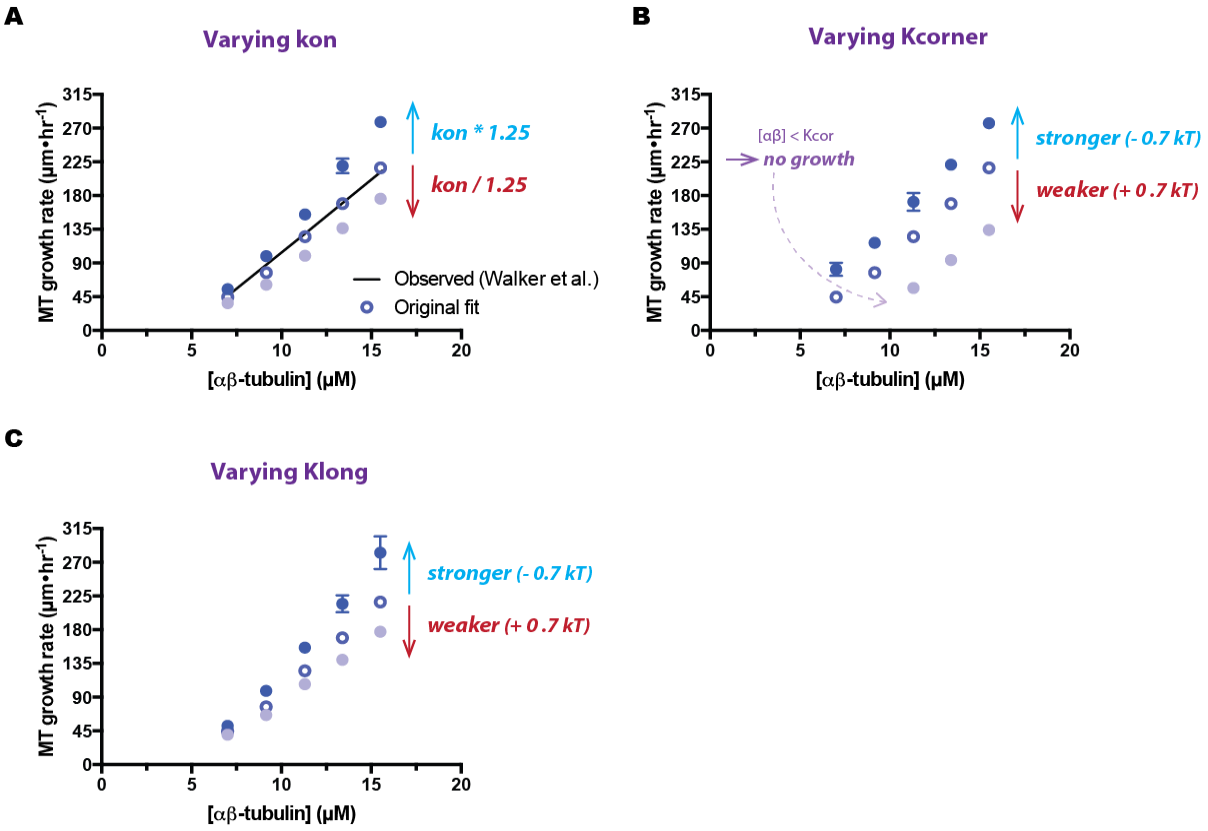

Figure 1. Rates of MT elongation depend on the on-rate constant (kon) and binding affinities.

(**A**) The kon affects the slope of concentration-dependent rates of MT elongation. A plot of MT growth rate (µm·hr^{-1}) vs. [αβ-tubulin] (µM) showing: 1) benchmark observations of porcine MT elongation rates ('Observed' [black line]) (Walker et al., 1988); 2) results from fitting our model to benchmark observations (kon = 4 µM^{-1}s^{-1}; Kcorner = 4.12 µM; Klong = 3.0 mM [open blue circles]); 3) results from increasing the kon in our model (kon = 1.25 * 4 µM^{-1}s^{-1} = 5 µM^{-1}s^{-1} [closed blue circles]); and 4) results from decreasing the kon in our model (kon = 1/1.25 * 4 µM^{-1}s^{-1} = 3.2 µM^{-1}s^{-1} [closed lavender circles]). n =3 for each data point and error bars represent the standard deviation. Changing the kon by a factor of 1.25 up-or-down has the effect of increasing or decreasing the apparent kon (slope) by the same factor. (**B**) The corner binding affinity affects the offset of concentration-dependent rates of MT elongation. A plot of MT growth rate (µm·hr^{-1}) vs. [αβ-tubulin] (µM) showing: 1) results from fitting our model to benchmark observations of porcine MT elongation rates (kon = 4 µM^{-1}s^{-1}; Kcorner = 4.1 µM; Klong = 3.0 mM [open blue circles]); 2) results from decreasing (strengthening) Kcorner in our model by a factor of 2 (ΔG_{corner} - 0.7 kT) while keeping Klong constant (Kcorner = 2.05 µM [closed blue circles]); and 3) results from increasing (weakening) Kcorner in our model by a factor of 2 (ΔG_{corner} + 0.7 kT) while keeping Klong constant (Kcorner = 8.30 µM [closed lavender circles]). n =3 for each data point and error

bars represent the standard deviation. Changing Kcorner by a factor of 2 up-or-down mainly has the effect of changing the x-intercept (critical concentration): 1) stronger Kcorner (x-int = 8.25 μM; slope = 23 $\mu m \cdot hr^{-1} \mu M^{-1}$); 2) Kcorner unchanged (x-int = 5.11 μM ; slope = 21 $\mu m \cdot hr^{-1} \mu M^{-1}$); 3) weaker Kcorner (x-int = 3.81 μM; slope = 18 $\mu m \cdot hr^{-1} \mu M^{-1}$). Elongation is not possible at [αβ-tubulin] < Kcorner. (**C**) The longitudinal binding affinity affects the slope of concentration-dependent rates of MT elongation. A plot of MT growth rate ($\mu m \cdot hr^{-1}$) vs. [αβ-tubulin] (μM) showing: 1) results from fitting our model to benchmark observations of porcine MT elongation rates (kon = 4 $\mu M^{-1} s^{-1}$; Kcorner = 4.1 μM; Klong = 3.0 mM [open blue circles]); 2) results from decreasing (strengthening) Klong in our model by a factor of 2 (ΔG_{long} - 0.7 kT) while keeping Kcorner constant (Klong = 1.5 mM [closed blue circles]); and 3) results from increasing (weakening) Klong in our model by a factor of 2 (ΔG_{long} + 0.7 kT) while keeping Kcorner constant (Klong = 6.1 mM [closed lavender circles]). n =3 for each data point and error bars represent the standard deviation. Changing Klong by a factor of 2 up-or-down has the effect of increasing or decreasing the apparent kon (slope) by a factor of 1.3.

MT shrinking in our model results from the one by one loss of GDP-bound subunits from the MT lattice. Single subunits can dissociate from 1) corner, 2) longitudinal, or 3) bucket (1 longitudinal + 2 lateral) sites. We performed dilution experiments (see 'parameter optimization' section immediately above) to determine the extent to which the shrinking rate is sensitive to varying strengths of the preceding interaction types (Fig. 2). Results from our dilution experiments indicate that MT shrinking in our model is dominated by dissociations from corner sites.

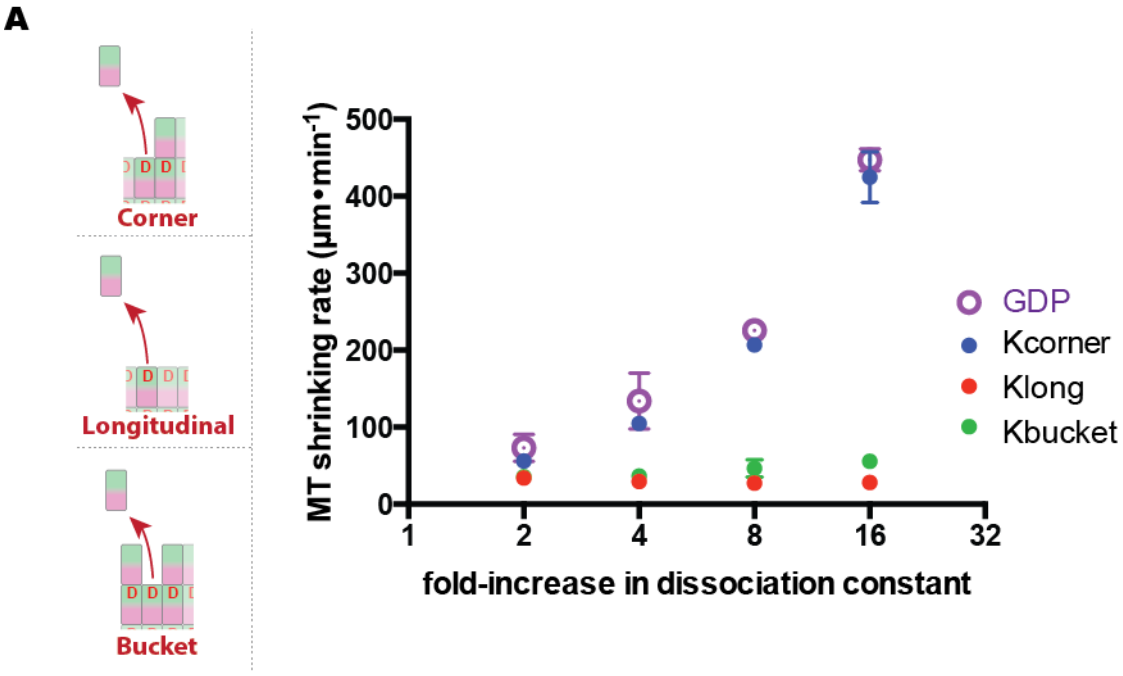

Figure 2. The rate of MT shrinking depends on the corner affinity and the GDP-weakening effect.

(**A**) (left) During MT shrinking, single subunits can dissociate from corner, longitudinal, or bucket sites. (right) A plot of MT shrinking rate ($\mu m \cdot min^{-1}$) vs. fold-increase in dissociation constant showing results from dilution experiments with: 1) increasing GDP-weakening effect (open purple circles); 2) weakening Kcorner (closed blue circles); 3) weakening Klong (closed red circles); and 4) weakening Kbucket (closed green circles). n =3 for each data point and error bars represent the standard deviation. The parent parameters-- i.e., 0-fold increase in dissociation constant (kon = 4 $\mu M^{-1}s^{-1}$; Kcorner = 4.12 μM; Klong = 3.0 mM; GDP = 35) give rise to a shrinking rate of 28 ± 1 μm/min.

Catastrophe is the most parameter-intensive feature of our model's output. We determined the extent to which the catastrophe frequency is sensitive to the following parameters by varying each independently: 1) the concentration of αβ-tubulin; 2) the rate of GTP hydrolysis; and 3) the rate of GDP to GTP exchange on the MT end (Fig. 3). The catastrophe frequency depends sensitively on the concentration of αβ-tubulin, increasing by a factor of 8 from 11 to 9 μM αβ-tubulin (Fig. 3A). The catastrophe frequency also depends sensitively on the rate of GTP hydrolysis; and an exponential growth function fits the dependence well (R^2 = 0.97) (Fig. 3B). The catastrophe frequency also varies with the rate of GDP to GTP exchange on the MT end, decreasing by a factor of 14 from an exchange rate of 0.2 to 2.0 s^{-1} at k_{GTPase} = 0.2 s^{-1} (Fig. 3C). Increasing the rate of GDP to GTP exchange on the MT end does not alter the exponential dependence of the catastrophe frequency on k_{GTPase}, however it does shift the curve to higher values of k_{GTPase} (Fig. 3B).

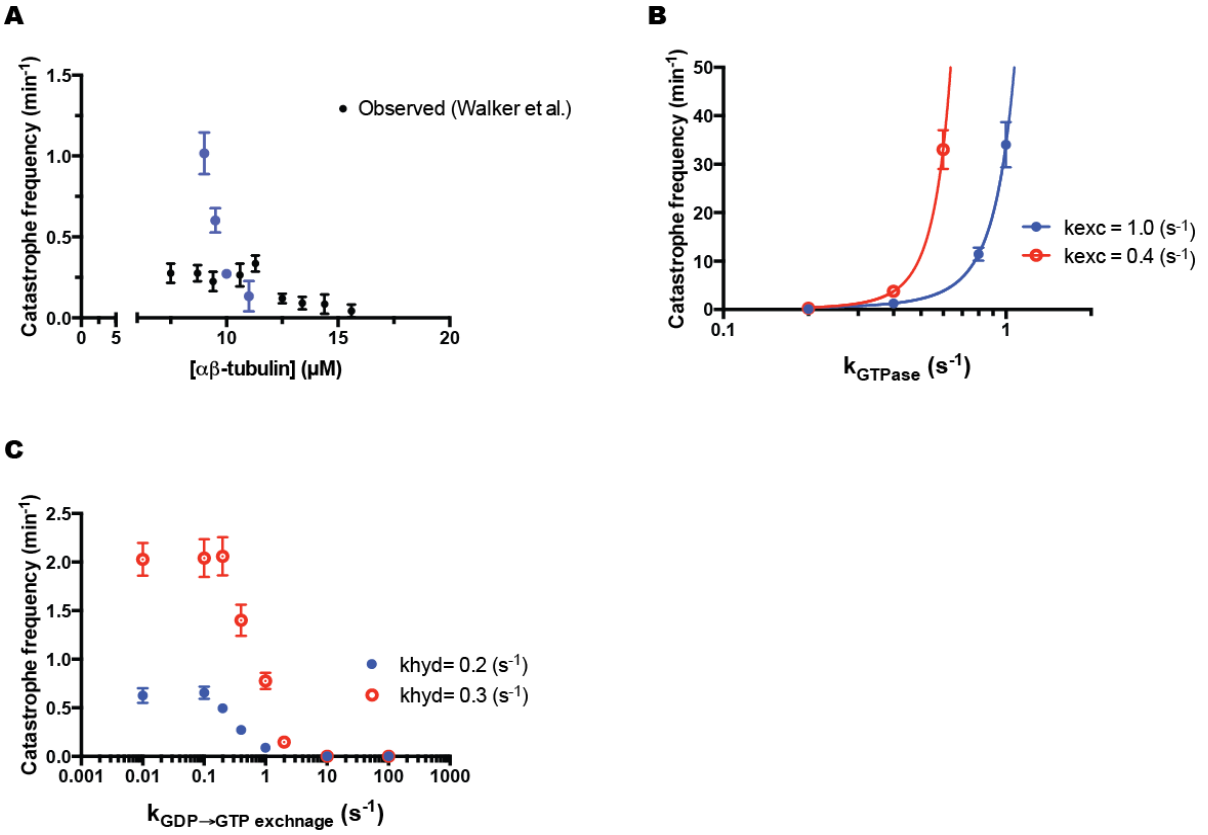

Figure 3. The catastrophe frequency depends sensitively on concentration and the GTPase rate, and also depends on the rate of GDP to GTP exchange on the MT end

(**A**) A plot of catastrophe frequency (min^{-1}) vs. [αβ-tubulin] (μM) showing 1) benchmark observations of porcine MT catastrophe frequencies (black dots) (Walker et al., 1988), and 2) results from our model (blue dots). Simulated catastrophe frequencies were acquired by fitting our model to the catastrophe frequency observed at one αβ-tubulin concentration, fixing our parameters and varying the αβ-tubulin concentration simulated from 11 to 9 μM in 0.5 μM increments (parameters: kon = 4 $\mu M^{-1}s^{-1}$; Kcorner = 4.12 μM; Klong = 3.0 mM; GDP = 35; k_{GTPase} = 0.2 s^{-1}; $k_{GDP\rightarrow GTP\ exchange}$ = 0.4 s^{-1}). From left to right, n = 11, 91, 65, 62; error bars represent the standard deviation. (**B**) A plot of catastrophe frequency (min^{-1}) vs. k_{GTPase} (s^{-1}) for two values of $k_{GDP\rightarrow GTP\ exchange}$ (0.4 [red] & 1.0 s^{-1} [blue]). An exponential growth function fits both data sets well (for $k_{GDP\rightarrow GTP\ exchange}$ = 0.4 s^{-1}: y_o = 0.05 min^{-1}; k = 10.89; R^2 =0.97; for $k_{GDP\rightarrow GTP\ exchange}$ = 1.0 s^{-1}: y_o = 0.15 min^{-1}; k = 5.45; R^2 =0.97). From left to right, for $k_{GDP\rightarrow GTP\ exchange}$ = 0.4 s^{-1} (red), n = 91, 130, 52; from left to right, for $k_{GDP\rightarrow GTP\ exchange}$ = 1.0 s^{-1} (blue), n = 11, 77, 88, 53; error bars represent the standard deviation. (**C**) A plot of catastrophe frequency (min^{-1}) vs. $k_{GDP\rightarrow GTP\ exchange}$ (s^{-1}) for two values of k_{GTPase} (0.2 [blue] & 0.3 s^{-1} [red]). From L to R for k_{GTPase} = 0.2 s-1 (blue): n = 68, 109, 108, 91, 11, 0, 0; from L to R for k_{GTPase} = 0.3 s-1 (magenta): n = 144, 110, 86, 16, 0, 0; error bars represent the standard deviation.

Protein expression and purification

Plasmids to express wild type yeast αβ-tubulin have been described previously (Johnson et al., 2011; Ayaz et al., 2012) and were used without further modification. Plasmids encoding the C12A and C12S mutants were generated by site-directed mutagenesis. The integrity of constructs was confirmed by sequencing.

Wild type and mutant yeast αβ-tubulin were overexpressed in *S. cerevisiae* (Johnson et al., 2011). All proteins were purified using Ni-affinity and anion exchange chromatography as described previously (Johnson et al., 2011; Ayaz et al., 2012), dialyzed into storage buffer (10 mM PIPES pH 6.9, 1 mM MgSO4, 1 mM EGTA) containing 50 uM GTP (for polymerization measurements) or 50 uM GDP (for binding assays; GDP is not bound as tightly and is therefore easier to displace).

Binding assays

Wild type or mutant yeast αβ-tubulin in 50 μM GDP was taken from -80 deg. C, rapidly thawed, and passed through a Millipore 0.1 μm centrifugal filter at 12000 g for 4 min at 4 deg. C. Filtrate was then passed over a Nick Sephadex G-50 gravity desalting column into buffer containing 10 mM PIPES, 1 mM EGTA, and 1 mM $MgSO_4$ in order to remove free GDP and GDP bound to the e-site of αβ-tubulin. A control experiment wherein ion exchange chromatography was used to quantify the nucleotide content of the treated tubulin showed that this procedure removes ~90% of the exchangeable nucleotide (data not shown). The

concentration of αβ-tubulin in the filtrate was measured by UV absorbance using an extinction coefficient of 106835 $M^{-1}cm^{-1}$ (assuming all of the exchangeable GDP was removed).

To measure the affinity of S^6-GTP for αβ-tubulin, we prepared 220 µl samples containing either 0.16 µM wild type or mutant αβ-tubulin (prepared as described above), 0.5% Tween-20, and a variable concentration of S^6-GTP in buffer containing 10 mM PIPES, 1 mM EGTA, and 1 mM $MgSO_4$. Samples were kept in Eppendorf Protein LoBind tubes and allowed to equilibrate to RT before measurement.

To measure the affinity of GDP or dGDP for αβ-tubulin, we prepared 220 µl samples containing either 0.16 µM wild type or mutant αβ-tubulin (prepared as described above), 0.5% Tween-20, 5 µM S^6-GTP, and variable concentrations of GDP or dGDP, in buffer containing 10 mM PIPES, 1 mM EGTA, and 1 mM $MgSO_4$.

Measurements of fluorescence quenching by S^6-GTP and unquenching by GDP or dGDP were made in 96 well flat bottom black polystyrene plates using a Thermo Scientific Varioskan FLASH plate fluorimeter. 200 µl of each sample (including a blank) were loaded per well. Tryptophan fluorescence from αβ-tubulin was excited at 296 nm using a 12 nm slit width. Emission was monitored at 329 nm, with dynamic range set to medium high and a measurement time of 80 ms. Each sample was measured 100 times and mean fluorescence intensities were calculated. Experiments were repeated multiple times on different days.

Results from each experiment were used to calculate the reported mean fluorescence and standard error values.

Because S^6-GTP absorbs strongly at tryptophan's emission peak, and both GDP and dGDP absorb at the excitation wavelength, it was necessary to correct our experiments for the inner filter effect (Fishback and Yarbrough, 1984). To accomplish this we measured fluorescence from buffer samples containing ~50 μg/ml BSA and a variable concentration of S^6-GTP or GDP (GDP and dGDP have the same UV absorbance spectra, so only one had to be measured). The concentration of BSA was chosen to give the same fluorescence intensity as 0.16 μM αβ-tubulin. Each sample was measured as described above, and mean fluorescence and standard error values were calculated. An exponential decay function weighted by the standard errors was fit to the mean fluorescence intensity values of each titration series (S^6-GTP or GDP) and used to calculate correction factors that were later applied to the raw intensities recorded in quenching and unquenching experiments. For S^6-GTP quenching experiments, we corrected fluorescence emission data using the expression Fcorrected = Fobserved*EMcorrection([S6-GTP]). Where 'EMcorrection' is the inner filter correction for emission determined at different concentrations of S6-GTP. For GDP or dGDP competition experiments we corrected fluorescence emission data using the expression Fcorrected = Fobserved*EMcorrection(5 uM S6-GTP)*EXcorrection([GDP]), where 'EXcorrection' is the inner filter correction for excitation determined at various concentrations of GDP.

To quantify the affinity of αβ-tubulin for S^6-GTP, we fit the fluorescence signals measured from the S^6-GTP titration to a single-site saturation binding curve (accounting for ligand depletion, and weighted by the standard errors) (GraphPad Prism version 6). To determine the affinity of αβ-tubulin for competing nucleotide (GDP or dGDP), we fit the Cheng-Prusoff equation ($F_u = x / (x + K_i(1 + (L_T/K_D)))$), where F_u = fraction unquenched, x = concentration of competing nucleotide, K_i = dissociation constant for competing nucleotide, L_T = total concentration of S6-GTP, K_D = dissociation constant for S6-GTP) {Cheng:1973wh} weighted by the standard errors to the normalized fluorescence signals measured from the titration of the competing nucleotide.

Time-lapse measurements of microtubule dynamics

Flow chambers were prepared as described previously (Gell et al., 2010), with the exception that sea urchin axonemes were used to template yeast MT growth (Waterman-Storer, 2001). Sea urchin axonemes were adsorbed directly to treated coverglass before the blocking step.

Wild type or mutant yeast αβ-tubulin in 50 μM GTP was taken from -80 deg. C and rapidly thawed. Thawed sample was passed through a 0.1 μm centrifugal filter at 12000 g for 4 min at 4 deg. C. to remove aggregated αβ-tubulin resulting from freeze-thaw. The concentration of αβ-tubulin in the filtrate was measured by UV absorbance using an extinction coefficient of 115000 $M^{-1}cm^{-1}$ to account for two bound guanine nucleotides. Protein was kept on wet ice for no more than 30 minutes before use in a MT dynamics assay. MT dynamics reactions were imaged by differential interference contrast microscopy (DIC) using an Olympus IX81

microscope with a Plan Apo N 60x/1.42 NA objective lens and DIC prisms. Illumination was at 550 nm, obtained by inserting a 550 nm bandpass filter in the light path. Reactions were maintained at 30 deg. C by a WeatherStation temperature controller fit to the microscope's body. Micro-Manager 1.4.16 (Edelstein et al., 2010) was used to control the microscope and a Hamamatsu ORCA-Flash2.8 CMOS camera used to record the reactions. Movies of MT dynamics were recorded by taking an image every 500 ms for 1 to 2 hrs. At the end of each movie, a set of 100 out-of-focus background images was taken for background subtraction (see below).

Image processing

To improve signal to noise, we averaged every 10 raw images using a script we wrote in ImageJ (Schneider et al., 2012). The averaged images were opened as a stack and their intensities were normalized. An averaged background image was then subtracted from each image in the stack. MT length was measured manually using a the PointPicker plugin for ImageJ. Rates of MT elongation and catastrophe frequencies were determined as described previously (Walker et al., 1988).

Results

We developed a kinetic Monte Carlo model to simulate microtubule polymerization dynamics one biochemical event (association, dissociation, GTP hydrolysis) at a time (Ayaz et al., 2014). Our model was inspired by, and is very similar to, one previously developed by Odde and Cassimeris (VanBuren et al., 2002), with the exception that we assume the

nucleotide acts in trans to regulate the strength of the longitudinal interface (Fig. 1A), not in cis to control the strength of the lateral interface. We did not attempt to parameterize the effects of different αβ-tubulin conformations because there is not yet a consensus about how to do so. To obtain model parameters that could recapitulate microtubule elongation and shrinking rates and approximate the frequency of catastrophe, we followed the approach outlined in (VanBuren et al., 2002)(Methods). Like this previous model, our model does not recapitulate 'age-dependent' catastrophe, perhaps because it does not account for different conformations of αβ-tubulin. Our parameter search yielded parameters comparable to those identified previously for the same data (VanBuren et al., 2002), validating our implementation (Figure 4).

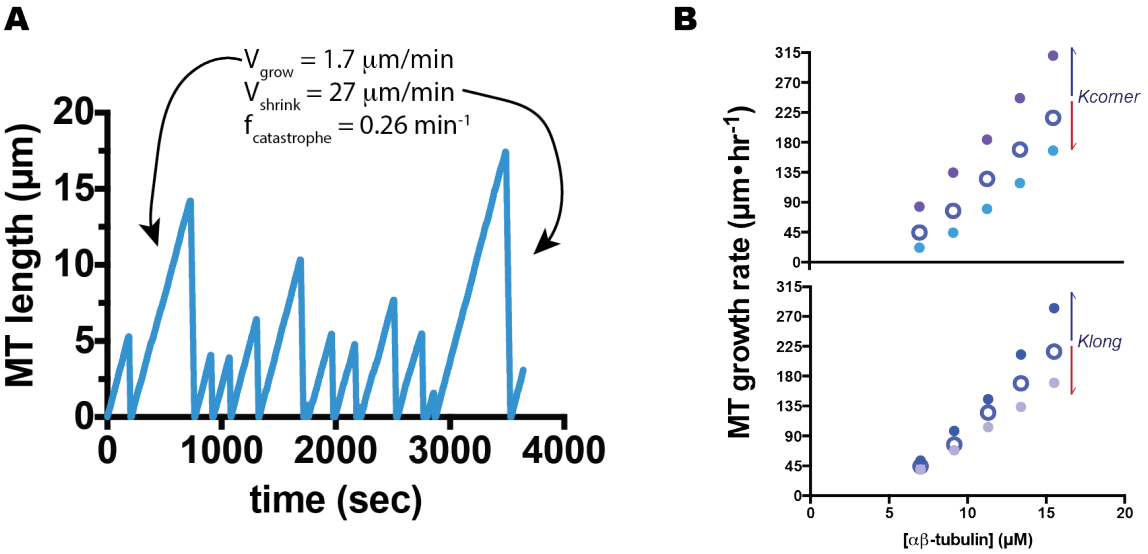

Figure 4. A kinetic Monte Carlo model where the nucleotide acts in trans reproduces benchmark observations of porcine MT elongation and shrinking rates.

A kinetic Monte Carlo model where the nucleotide acts in trans can reproduce benchmark observations of porcine MT elongation and shrinking rates. **(A)** A plot of MT length vs. time showing results from a simulation with parameters tuned to reproduce the Walker et al. data. Growing and shrinking rates are obtained from average slopes of the appropriate segments, and the frequency of catastrophe is calculated as the number of catastrophes divided by the total time spent growing. Our simple model captures the concentration-dependence of elongation rates; it also recapitulates the frequency of catastrophe at 10 μM αβ-tubulin, but like a similar prior model ours shows a too-steep concentration-dependence of catastrophe.The following parameters were used: k_{on} = 4 $\mu M^{-1}s^{-1}$; $K_{longitudinal}$ = 3 mM; $K_{longitudinal+lateral}$ = 3.1 mM; weakening effect of GDP on the longitudinal interface = 78.75-fold (see Methods). Parameter values are comparble to those used by Vanburen et al. to fit the same data (Kcorner = 3.7 μM, Klong = 1.1 mM). **(B)** The longitudinal+lateral ('corner') and longitudinal affinities have different effects on the concentration-dependence of rates of MT elongation. Top: a plot of MT growth rate vs. [αβ-tubulin] shows that tightening or weakening K_{corner} while keeping K_{long} constant mainly alters the x-intercept (which is the apparent critical concentration) with little effect on the slope (which gives the apparent k_{on}). Bottom: a plot of MT growth rate vs. [αβ-tubulin] shows that tightening or weakening K_{long} while keeping K_{corner} constant alters the slope (apparent k_{on}) without significantly altering the x-intercept (apparent critical concentration).

During the parameter optimization we unexpectedly observed that simulated elongation rates decreased as the GTPase rate constant increased (Fig. 5B). We hypothesized that the simulated microtubules grew more slowly because GDP-tubulin was being exposed at the microtubule end, frustrating elongation. To test this idea, we performed simulations wherein terminal GDP-tubulin subunits were instantly converted to GTP-tubulin (Methods). These simulations gave elongation rates indistinguishable from those obtained without any GTPase activity (Fig. 5B), supporting the idea that occasional exposure of GDP-tubulin at the microtubule end caused the GTPase-induced slowdown in our model. These results led us to speculate that the rate of GDP to GTP exchange on terminal subunits might contribute to the frequency of catastrophe.

Interestingly, the earliest models for MT dynamics included a role for terminal nucleotide exchange (Chen and Hill, 1983; 1985). Terminal exchange was not retained in subsequent models (VanBuren et al., 2002; 2005; Brun et al., 2009; Bowne-Anderson et al., 2013; Margolin et al., 2012; Bayley et al., 1989), presumably because cis-acting GTP became the dominant paradigm (Melki et al., 1989; Wang and Nogales, 2005) (but see {Margolin:2012bh}, which began to explore trans-acting GTP). However, *in vitro* experiments have shown that the terminal nucleotide is exchangeable (Mitchison, 1993; Caplow and Shanks, 1995) and that modulating the amount of terminal GDP-tubulin exposure can alter the frequency of catastrophe (Caplow and Shanks, 1995; Vandecandelaere et al., 1995).

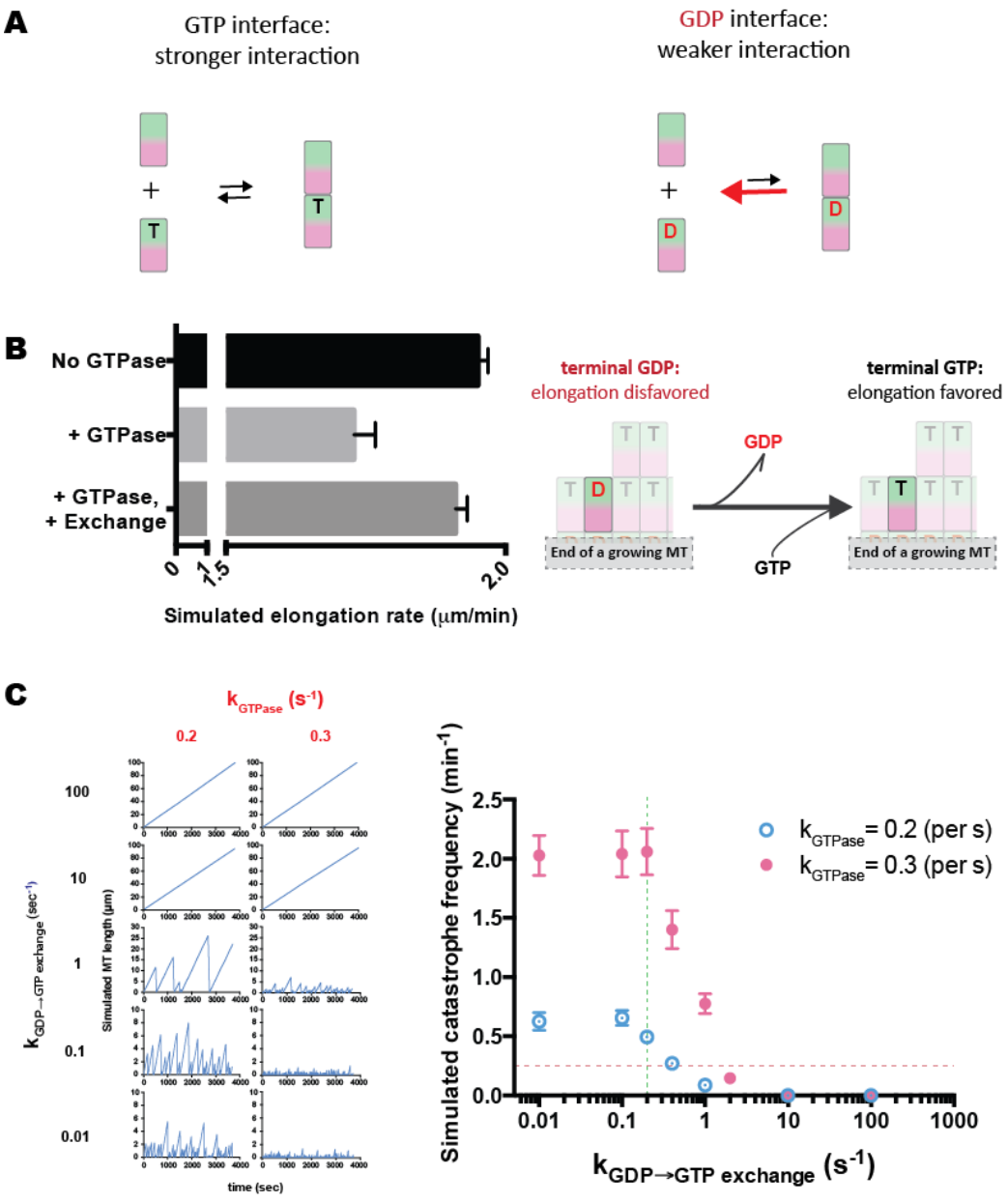

Figure 5. A potential role for GDP to GTP exchange in microtubule catastrophe is revealed by implementing trans-acting nucleotide into a Monte Carlo model of MT dynamics.

(A) Cartoon equilibria illustrating that trans-acting nucleotide modulates the strength of the longitudinal interface, with GDP giving weaker association. **(B)** (left) Introducing GTPase activity into the simulations resulted in a decrease in growth rate that could be rescued by instantaneous GDP to GTP exchange on the microtubule end. (right) The GTPase-induced

slowing of elongation and its rescue by GDP to GTP exchange can be understood because GDP exposure on the microtubule end frustrates growth compared to GTP. **(C)** (left) plots of MT length (μm) vs. time (sec) from simulations at 10 μM αβ-tubulin using two different values of kGTPase show that faster terminal nucleotide exchange suppresses the frequency of catastrophe. (right) a plot of catastrophe frequency (min-1) vs. kexchange (s-1) from simulations. (From L to R for kGTPase = 0.2 s-1 (blue): n = 68, 109, 108, 91, 11, 0, 0; from L to R for kGTPase = 0.3 s-1 (magenta): n = 144, 110, 86, 16, 0, 0; Error bars represent the standard deviation). The vertical green dashed line denotes the rate of exchange measured for unpolymerized αβ-tubulin {Melki:1988vb} ({Brylawski:1983vq} and {Yarbrough:1985vj} obtained similar values using different assays), and the horizontal red dashed line denotes the catastrophe frequency measured for 10 μM αβ-tubulin {Walker:1988ti}

To explore how the rate of GDP to GTP exchange on the microtubule end might affect the predicted frequency of catastrophe, we added this reaction to our algorithm assuming that GDP release was rate-limiting for exchange (Methods). We sampled a range of exchange rate constants in simulations, keeping other parameters fixed (Fig. 5C). Altering the rate of GDP to GTP exchange markedly affected the predicted frequency of catastrophe, with faster rates of exchange giving less catastrophe compared to slower rates (Fig. 5D).

A faster-exchanging αβ-tubulin mutant could provide a way to test the prediction that faster terminal exchange causes less frequent catastrophe. Directly measuring the rate of nucleotide exchange on the MT end is not yet possible, but we reasoned that a decrease in GTP/GDP binding affinity would lead to faster exchange. Accordingly, we sought to mutate GTP-interacting residues that do not participate in polymerization contacts or GTPase activity. The conserved β-tubulin residue C12 fits these criteria: the sidechain packs underneath the guanosine base of the exchangeable nucleotide, does not contact neighboring αβ-tubulins, and has not been implicated in catalysis (Fig. 6A). We therefore overexpressed and purified (Johnson et al., 2011) C12A yeast αβ-tubulin in order to study its GTP-binding and polymerization dynamics.

We measured the nucleotide binding affinity of C12A αβ-tubulin using a fluorescence-quenching assay (Amayed et al., 2000; Fishback and Yarbrough, 1984). The assay takes advantage of the fact that 6-thio-GTP (S^6-GTP) quenches the intrinsic fluorescence of αβ-tubulin when bound. We first determined the affinity of wildtype and C12A αβ-tubulin for

S^6-GTP, and then used a competition assay to obtain their affinity for GDP (Methods). C12A αβ-tubulin binds GDP with K_D = 6.5 μM; wildtype binds GDP less tightly, with K_D = 2.8 μM (Fig. 6B). A prior measurement of GTP binding to yeast αβ-tubulin showed higher affinity (~50 nM (Davis et al., 1993)); this discrepancy may be explained by the glycerol-free conditions we used (glycerol has been observed to increase the nucleotide binding affinity of αβ-tubulin (Yarbrough and Fishback, 1985)). Yeast αβ-tubulin shows some differences with vertebrate αβ-tubulin in terms of nucleotide binding: for example, the hydrolysis-resistant nucleotide GMPCPP that is widely used with vertebrate αβ-tubulin does not support the assembly of yeast αβ-tubulin (data not shown). We next measured the polymerization dynamics of this weaker-binding mutant using time-lapse differential interference contrast microscopy. C12A MTs showed growth rates comparable to wildtype albeit with somewhat lower concentration-dependence (Fig. 6B (left)), indicating that the mutation had at most a small effect on the strength of lattice interactions (see Fig 1). C12A MTs underwent catastrophe substantially less frequently than wildtype, showing a 6-fold difference at concentrations around 0.3 μM (Fig. 6B (right)). These results are consistent with the prediction that faster nucleotide exchange on terminal subunits leads to less frequent catastrophe.

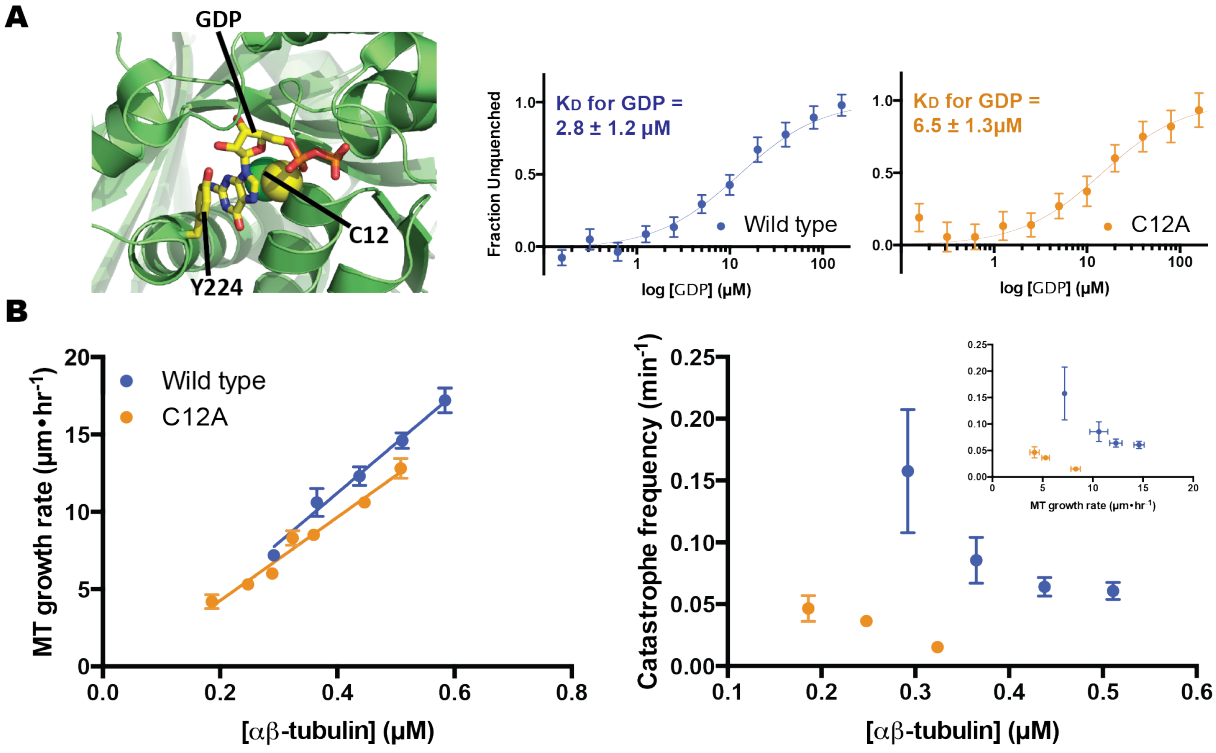

Figure 6. C12A yeast ab-tubulin binds less tightly to GDP, and C12A microtubules elongate comparably to wild-type but undergo catastrophe less frequently.

(A) C12 (sidechain represented as spheres) is a conserved residue that contacts the exchangeable GTP but that does not participate in polymerization contacts. The view in the left panel shows part of the surface that would be contacted by another ab-tubulin; Y224 shields the guanisine from polymerization contacts by stacking on top of it. PDB 4I4T {Prota:2013bd} was used for this illustration. The affinities of wild-type and C12A αβ-tubulin were measured using a fluorescence quencher displacement assay (see Methods). C12A yeast tubulin binds to GDP 2.3-fold less tightly than wild-type. (Each data point represents the mean fraction of signal restored at a particular concentration of GDP (n = 6 for wild -type; n = 7 for C12A); Error bars represent the standard error of the mean). **(B)** (left) C12A microtubules elongate comparably to wild-type, with a slight decrease in the concentration dependence (n=4 microtubules per data point, error bars show the standard deviation). Parameters (slope; x-intercept) from the linear regressions are: wild-type (33 +/- 1.9 µm/hr·µM; 0.06 +/- 0.03 µM) and C12A (27 +/- 1.8 µm/hr·µM; 0.04 +/- 0.02 µM). (right) C12A microtubules undergo catastrophe ~7-fold less frequently than wild-type. Inset: A plot of catastrophe frequency vs. MT growth velocity shows that the small changes in growth rate cannot explain the change in catastrophe frequency. (Each data point represents the catastrophe frequency measured at a particular concentration of αβ-tubulin (from L to R for wild type (blue): n = 10, 21, 75, 75; from L to R for C12A (orange): n = 20, 90, 63); Error bars represent the standard deviation).

Because the C12A measurements showed small changes in the concentration-dependence of elongation rates, we sought to identify a complementary way to alter the rate of terminal nucleotide exchange. Earlier work showed that deoxy analogs of GTP promote MT assembly while having reduced affinity for the e-site (Hamel et al., 1984). Structures of αβ-tubulin (e.g. {Prota:2013bd})further show (Fig. 7A) that the 2' hydroxyl group of the guanine nucleotide does not participate in polymerization contacts. Thus, dGTP should provide a way to obtain altered nucleotide binding without using a mutant. Using the competition assay described above, we determined that yeast αβ-tubulin binds dGDP about 1.8-fold less tightly than GDP (Fig. 7B), consistent with prior measurements using mammalian αβ-tubulin (Hamel et al., 1984). Measured elongation rates of MTs also changed very little in dGTP compared to GTP (Fig. 7B (left)), indicating that the removal of the 2'-OH did not perturb the strength of lattice contacts. Despite very similar rates of elongation, however, the catastrophe frequency decreased in the presence of dGTP (over 4-fold decrease at 0.3 μM) (Fig. 7B (right)). These dGTP experiments further support the idea that faster exchange on terminal subunits decreases the frequency of catastrophe.

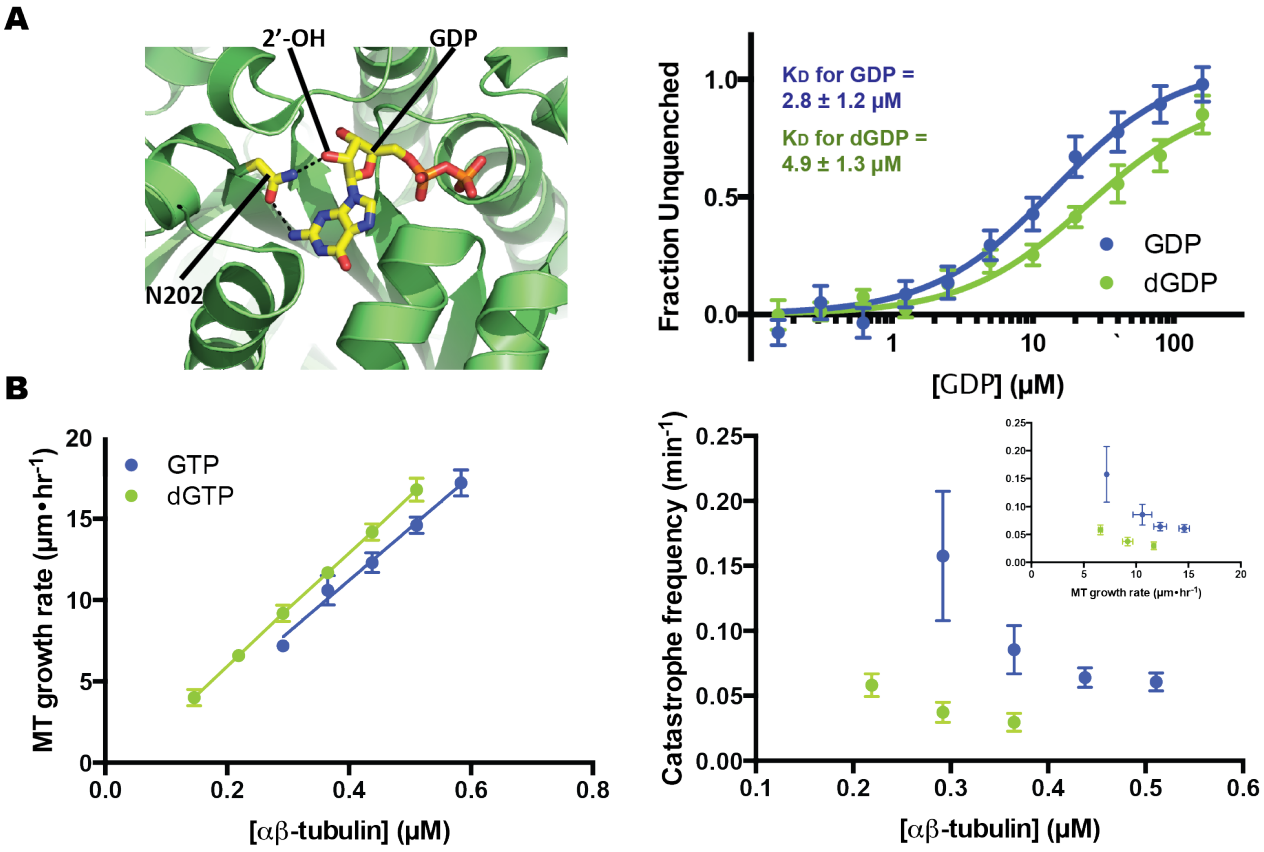

Figure 7. αβ-tubulin binds less tightly to 2'-deoxy GDP (dGDP) than to GDP, and polymerization in the presence of dGTP gives less frequent catastrophe than with GTP.

(A) (left) The 2' hydroxyl of GTP, which is absent in dGTP, makes a hydrogen-bond with a conserved asparagine (N202). PDB 4I4T {Prota:2013bd} was used for this illustration. (right) The affinities of yeast αβ-tubulin for GDP and dGDP were measured using a fluorescence quencher displacement assay (see Methods). αβ-tubulin binds to dGDP 1.8-fold less tightly than to GDP. (Each data point represents the mean fraction of signal restored measured at a particular concentration of GDP or dGDP (n = 6 for GDP (blue); n = 4 for dGDP (green)); Error bars represent the standard error of the mean). **(B)** (left) MTs assembled with dGTP elongate comparably to GTP MTs, with little change in the concentration dependence (n=4 MTs per data point, error bars show the standard deviation). Parameters (slope; x-intercept) from the linear regressions are: wild-type + GTP (33 +/- 1.9 μm/hr·μM; 0.06 +/- 0.03 μM) and wild-type + dGTP (35 +/- 0.1 μm/hr·μM; 0.03 +/- 0.001 μM). (right) MTs assembled with dGTP undergo catastrophe ~4-fold less frequently than with GTP. Inset: A plot of catastrophe frequency vs. MT growth velocity shows that the small increase in growth rate cannot explain the change in catastrophe frequency. (Each data point represents the catastrophe frequency measured at a particular concentration of αβ-tubulin (from L to R for wild-type + GTP (blue): n = 10, 21, 75, 75; from L to R for wild-type + dGTP (green): n = 43, 23, 18); Error bars represent the standard deviation).

To obtain more substantial perturbations of nucleotide-binding properties, we attempted analogous measurements using C12S or 3'- or 2',3'-deoxyGTP. It was previously observed that the C12S mutation is lethal in yeast αβ-tubulin (Gupta et al., 2001), and that it substantially abolishes the nucleotide binding of yeast γ-tubulin (Gombos et al., 2013), Consistent with these results, the C12S mutation in yeast αβ-tubulin severely impacted nucleotide binding (data not shown). C12S αβ-tubulin also formed slow growing microtubules that did not undergo catastrophe (Fig. 8). Because of the substantial effect on elongation rates, C12S likely perturbs lattice interactions, so we did not analyze these data in more detail. 3'- and 2',3'-deoxyGTP bound much less tightly to yeast αβ-tubulin compared to 2'-dGTP (Fig. 9), but increased spontaneous nucleation made it difficult to measure growth rates.

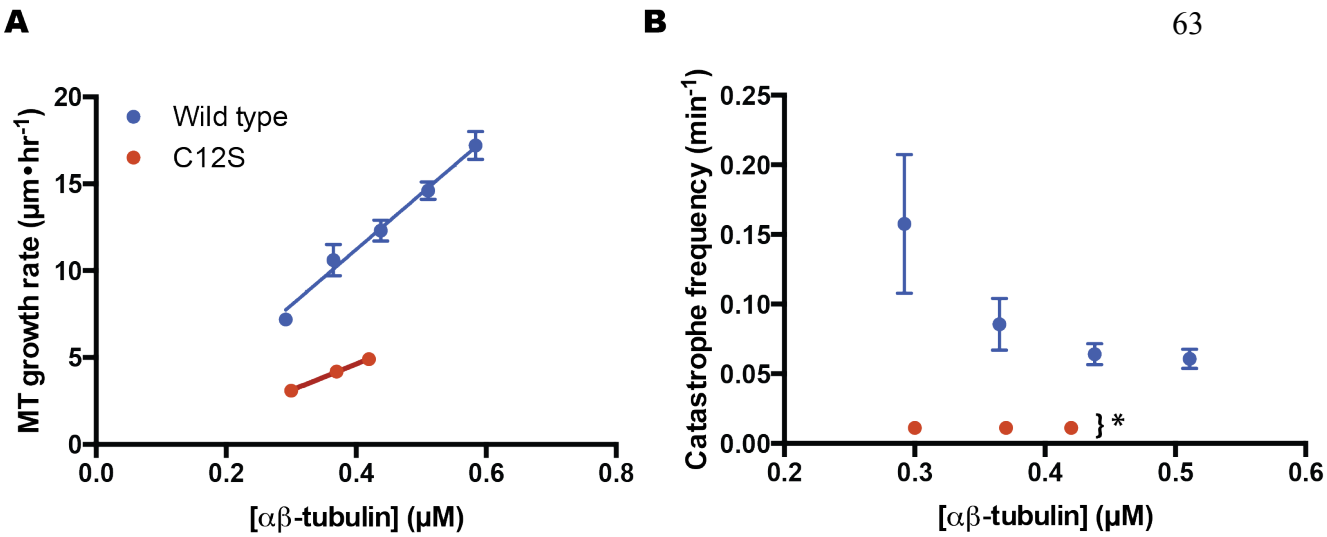

Figure 8. The C12S mutation suppresses catastrophe but also significantly affects rates of MT elongation.

(A) C12S microtubules elongate substantially slower than wild-type, mainly because of a decreased concentration-dependence (slope) (n=4 microtubules per data point, error bars show the standard deviation). Parameters (slope; x-intercept) from the linear regressions are: wild-type (33 ± 1.9 μm/hr·μM; 0.06 ± 0.03 μM) and C12S (15 ± 0.5 μm/hr·μM; 0.09 ± 0.01 μM). **(B)** A plot of catastrophe frequency vs. [αβ-tubulin] for C12S microtubules. (Each data point represents the catastrophe frequency in a single experiment at a particular concentration of αβ-tubulin (from L to R for wild type (blue): n = 10, 21, 75, 75; Error bars represent the standard deviation). The asterisk indicates that no catastrophes were recorded for C12S after 90 minutes of recording; therefore the plotted values only represent an upper limit on the true catastrophe frequency of C12S MTs.

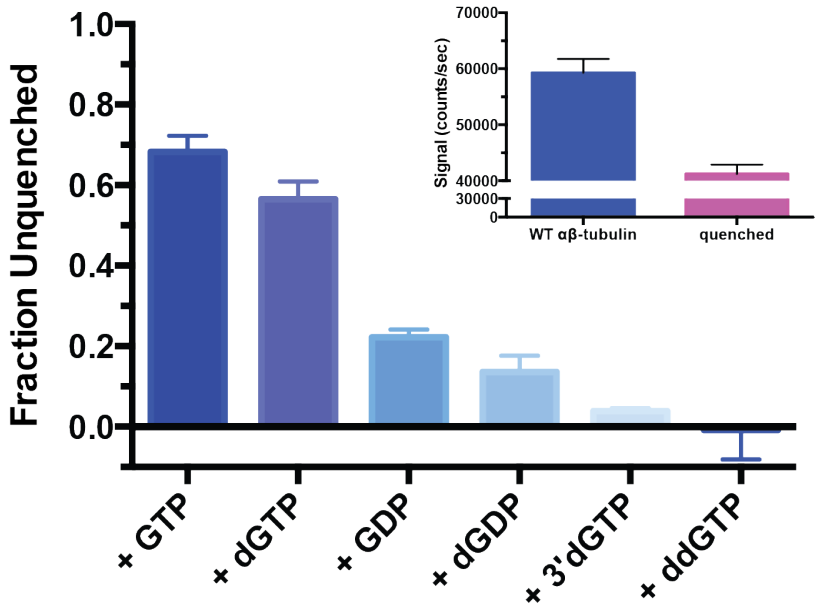

Figure 9. Deoxyguanosine nucleotides bind less tightly to yeast αβ-tubulin.

The bar chart quantifies the relative S6-GTP displacement efficiency of different nucleotides. Fraction unquenched is the amount of tryptophan fluorescence signal restored by displacement of quencher (S6-GTP, included at a concentration of 5 μM) by an equal concentration of competing nucleotide. Values of 0 and 1 represent no displacement and complete displacement, respectively. (Each data point represents the mean fraction of signal restored (n = 2 for all); Error bars represent the standard deviation). Inset: A bar chart showing the quenching by 5 μM S6-GTP in the absence of any competitor.

C12A αβ-tubulin, like wild-type, binds less tightly to dGTP than to GTP (Fig. 10A). Combining C12A and dGTP therefore provides an alternative way to further probe the relationship between the rate of nucleotide exchange and the frequency of catastrophe. When polymerized with dGTP, C12A microtubules underwent catastrophe about half as often as they did with GTP (Fig. 10B). The synergistic effect of the mutation and modified nucleotide thus provides additional support for a relationship between the frequency of catastrophe and the rate of GDP to GTP exchange on the microtubule end.

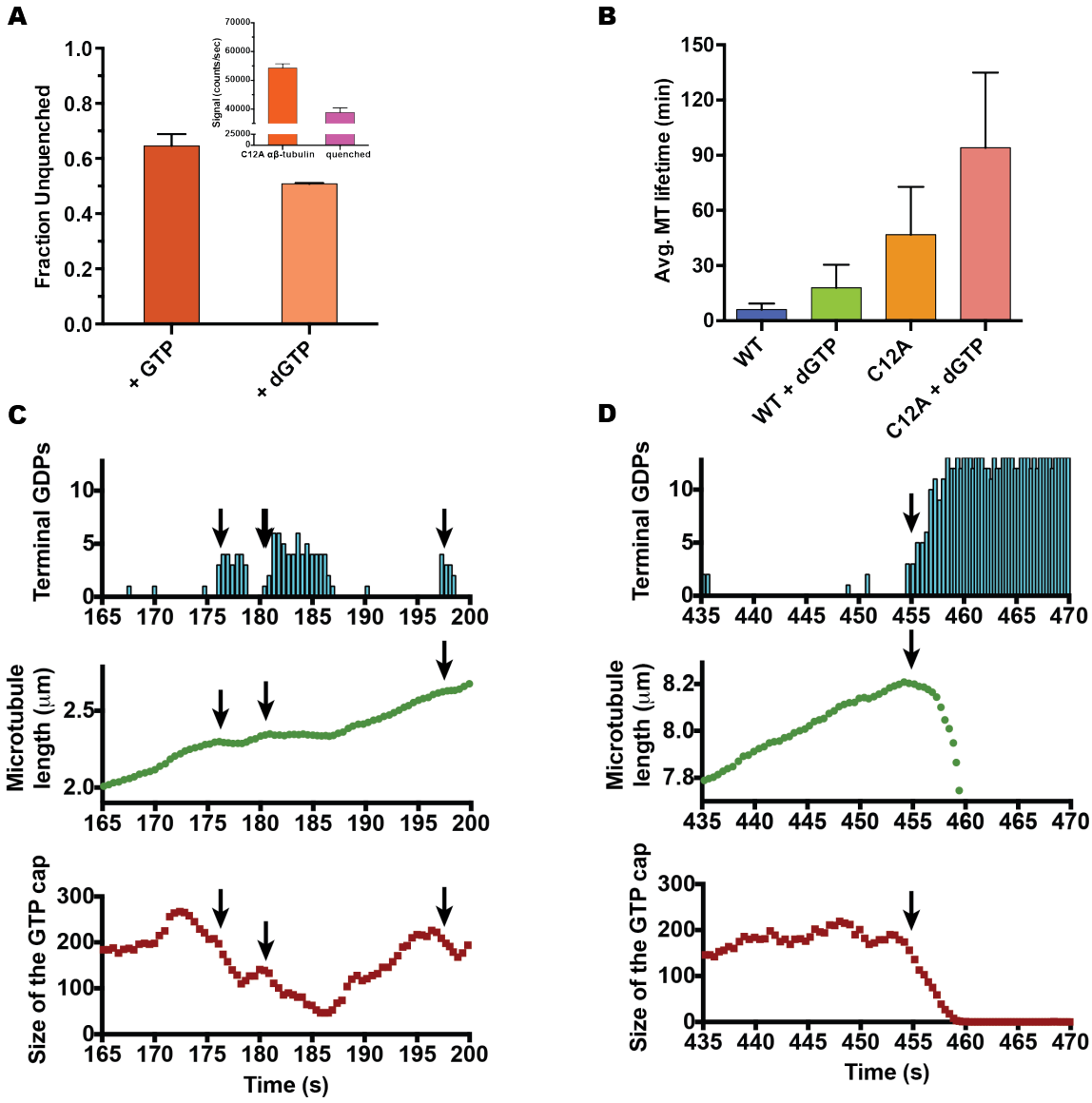

Figure 10. Exploring the effect of altered GDP to GTP exchange rates on MT catastrophe.

(A) C12A ab-tubulin binds less tightly to dGTP than to GTP. The plot shows that at equal concentration (5 mM), GTP is more effective than dGTP at displacing the fluorescence quenching nucleotide S6-GTP. The inset shows the raw fluorescence values before and after addition of S6-GTP. **(B)** The C12A and dGTP perturbations are synergistic: when growing in the presence of dGTP, C12A MTs undergo catastrophe less frequently than they do with GTP. The plot shows a histogram of average MT lifetime for wild-type and C12A yeast ab-tubulin polymerized with GTP or dGTP (for WT (blue): n = 10; WT + dGTP (green): n = 43; C12A (orange): n = 90; C12A + dGTP (coral): n = 44); Error bars represent the standard

deviation). Average MT lifetimes are for MTs growing at a rate of ~7 μm/hr. **(C)** GDP exposure can lead to transient pausing without catastrophe in our simulations. The number of terminal GDPs (top), the MT length (middle) and the size of the GTP cap (bottom) are all plotted versus simulation time. When GDP becomes exposed on the MT end (vertical arrows) in simulations, MT elongation slows down and the GTP cap starts to erode; subsequent restoration of GTP restores more normal growth rates and consequently the GTP cap is able to recover. Faster nucleotide exchange on the microtubule end contributes to increase the likelihood of these 'mini-rescues'. **(D)** Events leading to a catastrophe in our simulations. The number of terminal GDPs (top), the microtubule length (middle) and the size of the GTP cap (bottom; the cap fluctuates around its steady state value of about 190 under these conditions) are all plotted versus simulation time. When GDP becomes exposed on the microtubule end (vertical arrows), microtubule elongation slows down and the GTP cap is consumed, leading to rapid shrinking. The slowdown in growth and ensuing consumption of the cap are reminiscent of recent observations{Maurer:2014by}.

Discussion

Our results suggest that terminal nucleotide exchange is important to the molecular mechanisms of MT dynamics, and also provide a plausible (albeit partial) biochemical explanation for why microtubules occasionally exit otherwise sustained growth to undergo catastrophe. Recent work speculated that MT aging and catastrophe result from the essentially irreversible destabilization of a few protofilaments through exposure of GDP-bound αβ-tubulin at the MT end (Bowne-Anderson et al., 2013; Coombes et al., 2013). In our simulations with trans-acting GTP, however, GDP-terminated protofilaments are frequently exposed during sustained growth without necessarily causing catastrophe (Fig. 4D). GDP-terminated protofilaments eliminate favorable binding sites on the growing end, which in turn decreases the rate of elongation and leads to catastrophe by allowing GTP hydrolysis to erode the 'stalled' GTP cap (Fig. 4C). By converting some of these unfavorable binding sites back to favorable ones, GDP to GTP exchange can extend growth lifetimes by restoring normal growth rates and preventing further erosion of the GTP cap.

Microtubules were recently observed to pause and lose their EB1 comets, which mark the stabilizing cap, shortly before catastrophe (Maurer et al., 2014). The GDP-induced slowing of growth and accompanying loss of the GTP cap that we observe in our simulations are reminiscent of, and may explain, those events. The impossibility of GDP exposure at the minus-end might also explain the lower catastrophe frequency observed for minus-end MTs in vitro. More broadly, we speculate that a regulatory factor might modulate the frequency of catastrophe by tuning the rate of terminal GDP to GTP exchange on the microtubule end.

CHAPTER THREE

Comparing Microtubule Dynamics from Divergent αβ-tubulins

Abstract

Microtubules are dynamic polymers of αβ-tubulin that have essential roles in chromosome segregation and organizing the cytoplasm. MT dynamics can be reconstituted in vitro and monitored by various forms of optical microscopy. Numerous in vitro studies making use of αβ-tubulin purified from bovine or porcine brain have contributed immensely to our current understanding of MT dynamics, but scant attention has been paid to divergent αβ-tubulins; partly as a result of this, much remains unknown about how the biochemical properties of single αβ-tubulin subunits give rise to microtubule dynamics. We reconstituted MT dynamics from recombinant yeast αβ-tubulin and made measurements across a 2-fold range of concentrations. Yeast MT dynamics are strikingly different from porcine: yeast MTs polymerize at substantially lower concentrations of αβ-tubulin and elongate from plus-ends only, yet they shrink 5-fold faster. We fit a computational model to our data in order to begin to understand the molecular origins of these differences.

Introduction

Microtubules are essential to organisms across Eukaryota (from yeast to flies to people), and their component protein, αβ-tubulin, is highly conserved (Neff et al., 1983, Schatz et al., 1986). Nevertheless, variants of αβ-tubulin can give rise to microtubules that vary both structurally and dynamically, and these differences can play a significant role in vivo (Detrich et al., 2000; Pucciarelli et al., 2012; Sirajuddin et al., 2014). In vitro reconstitutions using variants of αβ-tubulin could help to elucidate the consequences of sequence and biochemical variation on MT dynamics, and in so doing improve our general understanding of MT dynamics.

To date the vast majority of in vitro measurements have been made using mammalian αβ-tubulin purified from bovine or porcine brain (Walker et al., 1988; Gardner et al., 2011b; Zanic et al., 2013), while little attention has been paid to non-mammalian αβ-tubulins. Gupta et al. measured yeast MT dynamics at a single concentration of αβ-tubulin (Gupta et al., 2002). Using a simple model, measurements of MT dynamics at multiple concentrations can be analyzed for biochemical rate constants like the apparent on-rate constant of GTP-bound αβ-tubulin and the apparent off-rate of GDP-bound αβ-tubulin (Walker et al., 1988). Measurements of MT dynamics across a range of αβ-tubulin concentrations therefore offer insight into the underlying biochemistry of αβ-tubulin:αβ-tubulin interactions (Walker et al., 1988). To enable a biochemical comparison of microtubule dynamics from divergent αβ-tubulins, we measured the concentration-

dependence of elongation rates and the rate of rapid shrinking from both yeast and porcine microtubules across a 2-fold range of concentrations and at two temperatures. We also measured the concentration-dependence of the catastrophe frequency from yeast MTs at a single temperature. We then fit a computational model of MT dynamics to our yeast and porcine data gathered at 30 °C.

Methods

Protein expression and purification

Plasmids to express wild type yeast αβ-tubulin have been described previously (Johnson et al., 2011; Ayaz et al., 2012) and were used without further modification.

Wild type yeast αβ-tubulin was overexpressed in *S. cerevisiae* and purified using Ni-affinity and anion exchange chromatography as described previously (Johnson et al., 2011; Ayaz et al., 2012), dialyzed into storage buffer (10 mM PIPES pH 6.9, 1 mM MgSO4, 1 mM EGTA) containing 50 μM GTP.

The lab of David Agard (UCSF) generously provided αβ-tubulin purified from porcine brain. Porcine αβ-tubulin was cycled into storage buffer following a publicly available protocol (Koshland).

Axoneme purification

Axonemes were purified from purple sea urchin (*S. purpuratus*) sperm following a published protocol (Waterman-Storer, 2001). Sea urchins were purchased from Gulf Specimen Marine Laboratories, Inc.

Time-lapse measurements of microtubule dynamics

Flow chambers were prepared as described previously(Gell et al., 2010), with the exception that sea urchin axonemes were used to template yeast MT growth (Waterman-Storer, 2001). Sea urchin axonemes were adsorbed directly to treated coverglass before the blocking step.

Wild type yeast αβ-tubulin in 50 µM GTP was taken from -80 deg. C and rapidly thawed. Thawed sample was passed through a 0.1 µm centrifugal filter at 12000 g for 4 min at 4 deg. C. to remove aggregated αβ-tubulin resulting from freeze-thaw. Protein was kept on wet ice for no more than 30 minutes before use in a MT dynamics assay. MT dynamics reactions were imaged by differential interference contrast microscopy (DIC) using an Olympus IX81 microscope with a Plan Apo N 60x/1.42 NA objective lens and DIC prisms. Illumination was at 550 nm, obtained by inserting a 550 nm bandpass filter in the light path. Reactions were maintained at 30 or 37 deg. C by a WeatherStation temperature controller fit to the microscope's body. Micro-Manager 1.4.16 (Edelstein et al., 2010) was used to control the microscope and a Hamamatsu ORCA-Flash2.8 CMOS camera used to record the reactions. Movies of MT dynamics were recorded by taking an image

every 500 ms for 1 to 2 hrs. At the end of each movie, a set of 100 out-of-focus background images was taken for background subtraction (see below).

Image processing

To improve signal to noise, we averaged every 10 raw images using a script we wrote in ImageJ (Schneider et al., 2012). The averaged images were opened as a stack and their intensities were normalized. An averaged background image was then subtracted from each image in the stack. MT length was measured manually using the PointPicker plugin for ImageJ. Rates of MT elongation and catastrophe frequencies were determined as described previously (Walker et al., 1988).

Results

Using a DIC-based assay, we measured rates of elongation and shrinking for yeast and porcine microtubules at 30 °C and across a 2-fold range of αβ-tubulin concentrations. In order to gain biochemical insight from our observations we analyzed our data using a one-dimensional model (Fig. 1A). Consistent with prior observations (Gupta et al., 2002), yeast αβ-tubulin polymerizes into microtubules at substantially lower concentrations than porcine αβ-tubulin (critical concentration of yeast αβ-tubulin = 0.06 μM, critical concentration of porcine αβ-tubulin = 1.56 μM) (Fig. 1B). The critical concentration reflects the affinity of αβ-tubulin for the MT end. Thus, the difference between yeast and porcine critical concentrations suggests that yeast αβ-tubulin has a higher affinity for the MT lattice than porcine αβ-tubulin when bound to GTP. The concentration-dependence

of MT elongation rates can be analyzed for an apparent on-rate constant (apparent kon) (Fig. 1B). The apparent kon defines the concentration-dependent rate of *productive* association of αβ-tubulin with the MT lattice; where the term 'productive' is used to distinguish association events leading to incorporation of αβ-tubulin into the growing MT lattice from the many transient binding events that occur during MT elongation. A mixture of transient and productive binding events is the consequence of a mixture of binding sites on the MT end, some weak and some strong (Fig. 2). Thus, the apparent kon is a single value that represents the average behavior of an elongating MT. Yeast αβ-tubulin polymerizes with an apparent kon (= 14.8 ± 0.9 $\mu M^{-1}sec^{-1}$) that is 4.5-fold higher than that of porcine αβ-tubulin (= 3.3 ± 0.3 $\mu M^{-1}sec^{-1}$) (Fig. 1B). The similarity of yeast and porcine αβ-tubulin makes it unlikely that they diffuse with different diffusion constants; therefore, the difference in apparent kon most likely reflects a different average distribution of binding sites. Additionally, we find that yeast MTs in vitro undergo plus-end directed growth exclusively (single axonemes at all concentrations assayed seeded MT growth from one end only-- not both, as is the case with porcine MTs) (Fig. 3). Also consistent with published results (Gupta et al., 2002), yeast MTs shrink roughly 5-fold faster than porcine MTs, suggesting that yeast αβ-tubulin has a lower affinity for the MT lattice than porcine αβ-tubulin when bound to GDP (Fig. 1C). Thus, combined our MT elongation and shrinking data suggest that yeast αβ-tubulin polymerizes more readily than porcine αβ-tubulin when bound to GTP, yet depolymerizes more readily than porcine αβ-tubulin when bound to GDP. This difference might result from substitutions at the longitudinal interface that lead to stronger

interactions with GTP and weaker interactions with GDP. It might also result from substitutions that make the difference in curvature between curved and straight conformations greater for yeast αβ-tubulin than porcine αβ-tubulin, creating greater contrast between growing and shrinking yeast MT end structures, and thus allowing for both enhanced polymerization and enhanced GTP hydrolysis-dependent depolymerization.

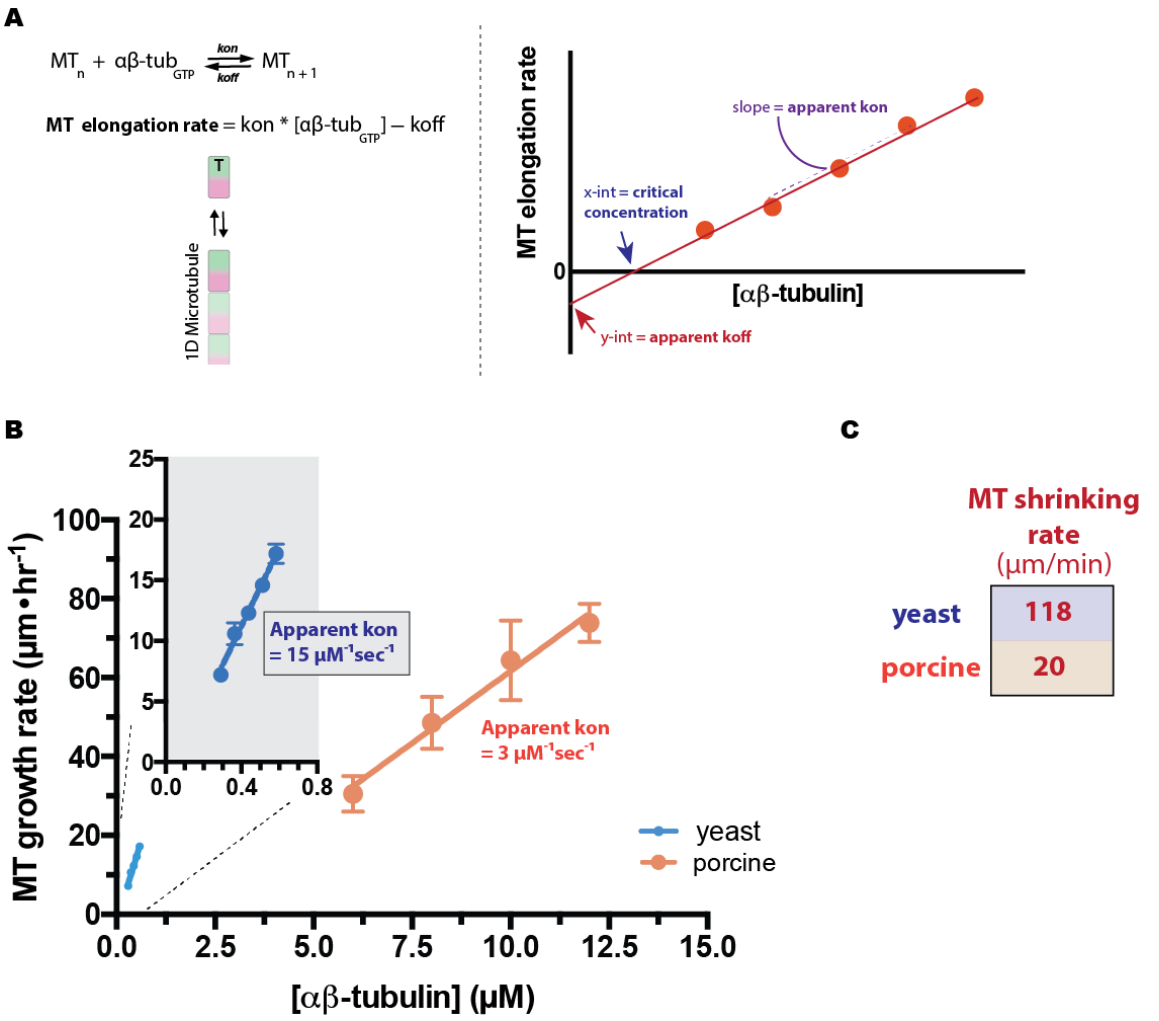

Figure 1. Yeast MTs polymerize and depolymerize more readily than porcine MTs.

(A) A one-dimensional (1D) model can be used to glean biochemical insight from observed rates of MT elongation. (left) A 1D model wherein subunit addition and dissociation occur to and from one site only predicts that MT elongation results from a simple equilibrium between polymerized (MT) and free GTP-bound αβ-tubulin (αβ-tub_{GTP}). (right) An example plot of MT elongation rate vs. [αβ-tubulin]. The red points depict hypothetical data. Several biochemical parameters are retrievable from a line fit to the data: 1) the apparent on-rate constant (apparent kon) = slope; 2) the apparent off-rate constant (apparent koff) = y-intercept; and 3) the critical concentration (apparent koff/apparent kon) = x-intercept. The term 'apparent' is used to make explicit the approximation made by fitting a 1D model to data collected from real MTs; each apparent rate constant can be thought of as an average over multiple types of interactions present at the ends of real MTs. **(B)** A plot of MT growth rate (μm/hr) vs. [αβ-tubulin] (μM) for yeast and porcine MTs observed at 30 °C. For yeast MTs (blue) and porcine

MTs (salmon) n=4 MTs per data point; error bars show the standard deviation. Parameters (slope; x-intercept) from the linear regressions are: yeast (14.8 ± 0.9 $\mu M^{-1}sec^{-1}$; 0.06 ± 0.03 μM) and porcine (3.3 ± 0.3 $\mu M^{-1}sec^{-1}$; 1.56 ± 0.6 μM). Slopes were converted into biochemical units (from μm/hr·μM to $\mu M^{-1}sec^{-1}$) by multiplying by 1625 (the number of αβ-tubulin subunits in 1 μm of MT) and dividing by 3600 (to convert hr^{-1} to sec^{-1}). **(C)** Yeast MTs shrink 5-fold faster than porcine MTs. A table of average MT shrinking rate (μm/min) for yeast and porcine MTs. Yeast and porcine MT shrinking rates are concentration-independent. (n = 15 MTs and n = 17 MTs were measured for the yeast and porcine shrinking rate, respectively)

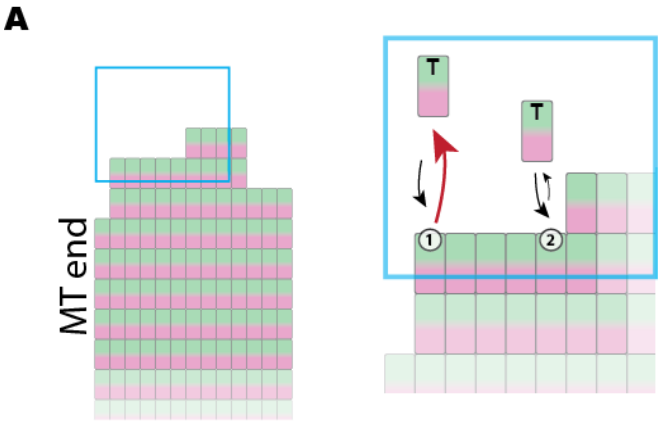

Figure 2. A mixture of binding sites exists on the MT end.

A mixture of transient and productive binding events is the consequence of a mixture of binding sites on the MT end. A cartoon depiction of the MT end showing two kinds of binding interactions: 1) longitudinal and 2) corner. The corner interaction is the stronger of the two because it involves two polymerization interfaces.

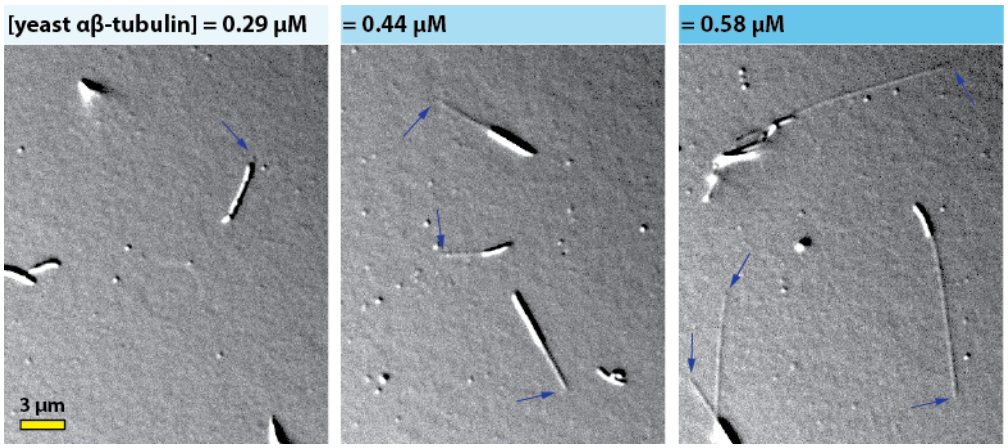

Figure 3. Yeast microtubules (MTs) in vitro elongate from plus-ends exclusively.

A panel of images taken by DIC microscopy of yeast MTs elongating off of axonemes in vitro. Images were taken ~45 minutes after the start of a reaction. (left) A blue arrow indicates the end of a small MT elongating at the lowest concentration of yeast αβ-tubulin assayed. (middle) Blue arrows indicate the ends of single microtubules and a bundle of microtubules (lowermost arrow) elongating at 0.44 µM. (right) Blue arrows indicate the ends of MTs elongating at the highest concentration of yeast αβ-tubulin assayed. Note: Images are sub-fields isolating single axonemes. Axonemes often cluster together in small groups of 3 or 4, and not all seed MT assembly (especially at lower concentrations of αβ-tubulin).

It has been known for decades that MT assembly/disassembly is strongly temperature-dependent (Inoue, 1951; Inoue, 1959; Inoue and Salmon, 1995). Fygenson et al. explored the effects of temperature on the individual parameters of dynamic instability using mammalian αβ-tubulin (Fygenson et al., 1994). Knowing how similarly or differently the polymerization behaviors of divergent αβ-tubulins depend on temperature might provide greater insight into the extent to which MT dynamics are conserved. We therefore wanted to compare the response to temperature change of both yeast and porcine MTs. To that end, we measured rates of MT elongation and shrinking at two different temperatures. From 30 to 37 °C, rates of yeast MT elongation did not change, while rates of porcine MT elongation increased significantly-- the apparent kon of porcine αβ-tubulin increased 2.2-fold (from 3.3 ± 0.3 $\mu M^{-1}sec^{-1}$ at 30 °C to 7.1 ± 0.4 $\mu M^{-1}sec^{-1}$ at 37 °C) (Fig. 4A). Published data show a similar effect for bovine MTs (from 19 to 30 °C, the apparent kon increased ~3-fold) (Fygenson et al., 1994). The strong temperature-dependence of the apparent kon suggests the existence of an activation barrier to polymerization. This activation barrier might result from the energetic cost of straightening weakly bound curved αβ-tubulin at the MT end during MT elongation. A recent study is consistent with this idea (Zanic et al., 2013). Zanic et al. found that two MT plus-end-binding proteins (XMAP215 and EB1) increase the rate of MT elongation synergistically through non-overlapping binding sites; they reasoned that the two worked allosterically to increase the isomerization rate of newly added αβ-tubulin from a weakly to a strongly bound form (curved to straight) (Zanic et al., 2013). However, the increase in apparent kon might also result from a temperature-dependent entropic effect involving water at a polymerization

interface. Furthermore, it is unclear why yeast microtubules did not show the same effect. Perhaps, assuming αβ-tubulin straightening underlies the temperature-sensitive apparent kon of porcine αβ-tubulin, yeast αβ-tubulin straightens more readily; or maybe yeast αβ-tubulin straightens as often, but a higher longitudinal affinity prevents straightening from being rate-limiting to MT elongation. It is also possible that, assuming the existence of an entropic effect involving water at a polymerization interface of porcine αβ-tubulin, substitutions at the relevant polymerization interface/s of yeast αβ-tubulin abrogate this effect. In contrast to the specific effect of temperature change on porcine MT elongation rates, the rate of rapid post-catastrophe shrinking for both yeast and porcine MTs increased approximately 2-fold from 30 to 37 °C (Fig. 4B). The shrinking rate of bovine MTs was observed to undergo a similar temperature-dependent increase (Fygenson et al., 1994). It is possible that the increase in yeast and mammalian MT shrinking rates results from a common temperature-dependent effect. Perhaps the rate of assembly-dependent GTP hydrolysis increases with temperature; this might lead to faster post-catastrophe shrinking by increasing the fraction of GDP-bound αβ-tubulin in the shrinking MT. Consistent with this idea, Tropini et al. found that 'islands' of GMPCPP (a nonhydrolyzable analog of GTP) slow the rate of post-catastrophe shrinking in porcine MTs (Tropini et al., 2012). Faster MT shrinking might also result from a temperature-dependent entropic effect involving water.

A

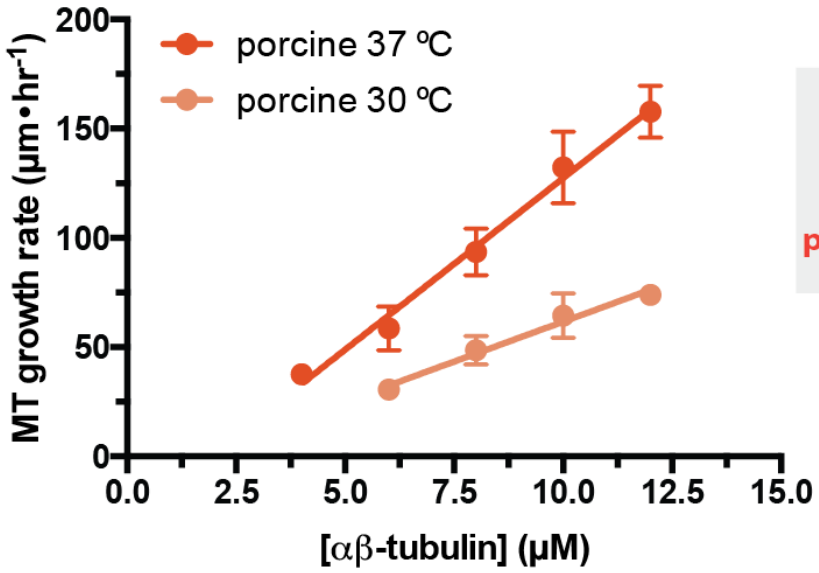

	Δ Apparent kon with T
yeast	none
porcine	2.2-fold

B

MT shrinking rate (µm/min)	30 ºC	37 ºC
yeast	118 ± 33	227 ± 17
porcine	20 ± 9	35 ± 21

Figure 4. Porcine MT elongation rates show temperature sensitivity from 30 to 37 °C

(A) Plot of MT growth rate (µm/hr) vs. [αβ-tubulin] (µM) showing data from plus-end growing MTs only. For porcine MTs at 37 °C (red) n=4 MTs per data point; for porcine MTs at 30 °C (salmon) n=4 MTs per data point; Error bars show the standard deviation. Parameters (slope; x-intercept) from the linear regressions are: porcine 37 °C (7.1 ± 0.4 $\mu M^{-1}sec^{-1}$; 1.9 ± 0.4 µM) and porcine 30 °C (3.3 ± 0.3 $\mu M^{-1}sec^{-1}$; 1.6 ± 1.4 µM). The slope of each linear regression is the apparent on-rate (app. kon), which is the rate of productive association of incoming αβ-tubulin subunits with the growing MT lattice. The apparent kon of porcine αβ-tubulin increases 2.2-fold from 30 to 37 °C, while over the same range the apparent kon of yeast αβ-tubulin shows no temperature dependence (data not shown). **(B)** Both yeast and porcine MT shrinking rates increase with temperature. A table of MT shrinking rate (µm/min) for yeast and porcine MTs at 30 and 37 °C. Yeast

and porcine MT shrinking rates are concentration-independent. (n = 15 MTs measured for the yeast shrinking rate at 30 °C; n = 7 MTs measured for yeast at 37 °C; n = 17 plus-end MTs measured for the porcine shrinking rate at 30 °C; n = 15 plus-end MTs measured for porcine at 37 °C.

We have relied mostly on a one-dimensional model to glean biochemical insight from our yeast and porcine MT dynamics data; but actual MTs are better approximated as two-dimensional objects. Two-dimensional models account for MT end structure and therefore allow for different kinds of αβ-tubulin interactions with the MT end, whereas one-dimensional models assume addition to and dissociation from one site only. Thus, to gain greater biochemical insight from our data, we fit our computational model for MT dynamics to rates of yeast and porcine MT elongation and shrinking collected at 30 °C.

We first searched for longitudinal and lateral binding constants needed to reproduce observed rates of yeast MT elongation. Simulations of MT assembly require specifying an intrinsic on-rate constant (kon) of free αβ-tubulin (where the intrinsic on-rate constant defines the rate of arrival of subunits onto each protofilament of the MT end). Both experimental and theoretical studies suggest that the value of this on-rate is around 1 to 10 $\mu M^{-1}sec^{-1}$ (Koren and Hammes, 1976; Northrup and Erickson, 1992). The authors of a previous study used a kon of 2 and 4 $\mu M^{-1}sec^{-1}$ to fit a similar model to benchmark observations of porcine MT dynamics collected at 37 °C (VanBuren et al., 2002). Assuming a kon of 2 $\mu M^{-1}sec^{-1}$ (Koren and Hammes, 1976; Northrup and Erickson, 1992), a Klong of 8 μM and a Kcorner of 9 nM reproduced rates of yeast MT elongation. Kcorner is the binding constant for a corner interaction (one longitudinal + one lateral). Because Klong is weak with respect to the concentrations of αβ-tubulin simulated (i.e., most pure longitudinal binding events are transient), elongation is dominated by addition

of single subunits to corner sites. A Klong of 8 μM would predict a large fraction of dimers around 1 μM αβ-tubulin (~30%), but we do not detect any dimers at this concentration by AUC or gel filtration (data not shown). Thus, we sought to identify alternative parameters with a higher (weaker) Klong. We observed previously that increasing the kon increases the Klong needed to capture observed rates of MT elongation (to keep elongation rates constant, weaker binding is needed to counter an increased binding rate). We therefore repeated our parameter search at a kon of 4 $\mu M^{-1} sec^{-1}$ and obtained a Klong of 34 μM and a Kcorner of 41 nM (Fig. 5A). At a Klong of 34 μM, dimers would represent less than 10% of the total free αβ-tubulin at 1 μM, making this Klong more realistic, although still on the tighter end of the longitudinal binding strength suggested by our AUC experiments.

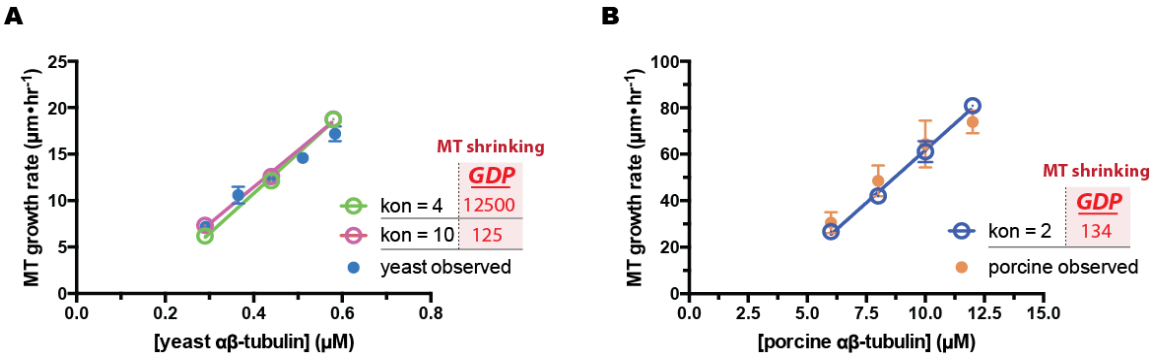

Figure 5. Our model captures both yeast and porcine MT dynamics data.

(A) (left) A plot of MT growth rate (μm/hr) vs. [yeast αβ-tubulin] (μM) showing our experimental observations (blue) and data from our model at two kons (kon = 4 $\mu M^{-1}s^{-1}$ [green]; kon = 10 $\mu M^{-1}s^{-1}$ [pink]). For both sets of simulated data, n = 5 MTs per data point; error bars show the standard deviation. To the right of each kon is the GDP-weakening factor needed to capture the observed rate of yeast MT shrinking **(B)** A plot of MT growth rate (μm/hr) vs. [porcine αβ-tubulin] (μM) showing our experimental observations (salmon) and data from our model at kon = 2 $\mu M^{-1}s^{-1}$ [blue). n = 5 MTs per data point; error bars show the standard deviation. To the right of the kon is the GDP-weakening factor needed to capture the observed rate of porcine MT shrinking

We searched for the GDP-weakening factor needed to reproduce the observed concentration-independent rate of yeast MT shrinking. To this end, we performed dilution experiments in silico: briefly, the aforementioned assembly parameters (kon = 4 $\mu M^{-1}sec^{-1}$; Klong = 34 μM; Kcorner = 41 nM) were used to simulate MT elongation to a length of 1 μm, after which the concentration of free αβ-tubulin was decreased to 0 μM, resulting in shrinking from the loss of GTP-bound subunits at the microtubule end; the fold-difference between this shrinking rate and the observed rate of rapid shrinking is the 'GDP-weakening' factor. We obtained a GDP-weakening factor of $1.25x10^4$ (Fig. 5A). This fold-difference in subunit binding affinity for GTP- and GDP-bound longitudinal interfaces seems unrealistically large. Knowing that a higher kon would permit weaker binding affinities to capture observed rates of yeast MT elongation (and thus a smaller GDP-weakening factor), we decided to refit our yeast data; we chose a kon of 10 $\mu M^{-1}sec^{-1}$ because this value is closer to the apparent kon. We obtained a Klong of 1.1 mM and a Kcorner of 34 nM (Fig. 5A). We then performed dilution experiments to obtain a GDP-weakening factor of 125 (Fig. 5A). This value, given its 100-fold smaller size, is more likely to fall within the realm of possibility. Simulations with a GDP-weakening factor of 125 and a GTPase rate constant of 0.04 sec^{-1} succeed in capturing the observed catastrophe frequency at 0.37 μM (Fig. 6).

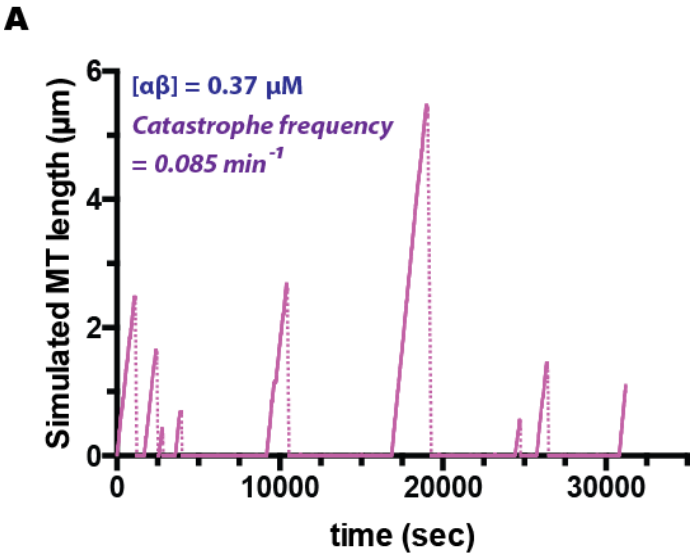

Figure 6. Our model captures the catastrophe frequency of yeast MTs at one concentration of αβ-tubulin

A plot of simulated MT length (μm) vs. time (sec). The following parameters were used to capture the observed catastrophe frequency (= 0.085 min^{-1}) at 0.37 μM αβ-tubulin: kon = 10 $\mu M^{-1}sec^{-1}$; Kcorner = 34 nM; Klong = 1.1 mM; GDP-weakening factor =125; kGTPase = 0.04 sec^{-1}.

For a comparison of yeast and porcine MT dynamics, we fit our model to porcine MT elongation and shrinking rates collected at 30 °C. We began by searching for longitudinal and lateral binding constants that reproduced rates of MT elongation. Shortly after commencing our parameter search, we realized that we could not fit both porcine and yeast MT elongation rates with the same kon (see discussion for a more thorough treatment of this matter). In our model, the kon used to capture any set of elongation rates can be at most equal to the apparent kon. Our porcine MTs assemble with an apparent kon of ~3 $\mu M^{-1}sec^{-1}$. We therefore began our parameter search at a kon of 2 $\mu M^{-1}sec^{-1}$, obtaining longitudinal and corner binding constants of 6.1 mM and 1.76 μM, respectively (Fig. 6B). A comparison of corner binding constants suggests that the affinity of porcine αβ-tubulin for the MT end is 50-fold weaker than that of yeast αβ-tubulin, comparable to the difference in affinities suggested by comparing their critical concentrations (the critical concentration of porcine αβ-tubulin is 26-fold higher-- 1.56 μM vs. 0.06 μM). Finally, we performed dilution experiments to obtain a GDP-weakening factor of 134 (Fig. 6B).

Discussion

Yeast and porcine MT dynamics differ markedly from one another. Yeast αβ-tubulin both polymerizes and depolymerizes more readily than porcine αβ-tubulin (26-fold lower critical concentration and 4.5-fold higher apparent kon, yet 5-fold faster MT shrinking). This difference might result from substitutions at the longitudinal interface that lead to

stronger interactions with GTP and weaker interactions with GDP. Our modeling results support this possibility. Enhanced yeast αβ-tubulin polymerization and depolymerization might also result from substitutions that make the difference in curvature between curved and straight conformations greater for yeast αβ-tubulin than porcine αβ-tubulin, creating greater contrast between growing and shrinking yeast MT end structures. We know from cryo-EM data (Chretien et al., 1995) that the growing and shrinking ends of porcine MTs are very different from one another structurally: the growing end is fairly straight (significantly, not completely-- see the MT structure and dynamics sections of Chapter 1), while the shrinking end has highly curved protofilaments that curl away from the MT body (Chretien et al., 1995). The protofilaments of shrinking yeast MTs might have a smaller radius of curvature at the MT end than their porcine equivalents; greater curvature could create deeper 'cracks' between protofilaments that would permit more rapid shrinking from the loss of longer oligomers of αβ-tubulin. Determining whether structural differences between growing and shrinking MT ends are amplified in yeast MTs would require imaging by cryo-EM.

Yeast MTs only undergo plus-end directed growth in vitro, while porcine MTs grow from both plus- and minus-ends. However, like yeast αβ-tubulin, it is somehow harder for porcine αβ-tubulin to productively bind the minus-end (Walker et al. observed a lower apparent kon from porcine minus-ends (we analyzed porcine plus-ends only)). But why should elongating from the minus-end be harder? Biochemical and structural evidence strongly suggest that free αβ-tubulin is curved independently of nucleotide-state (Buey et

al., 2006; Rice et al., 2008; Nawrotek et al., 2011), and we know that αβ-tubulin in the MT lattice is straight (Mandelkow et al., 1991; Chretien et al., 1995); thus, αβ-tubulin has to straighten at or near the MT end before incorporation into the MT lattice. We infer that αβ-tubulin straightening at the minus-end occurs at a slower rate than straightening at the plus-end for both yeast and porcine αβ-tubulin.

Yeast and porcine MT elongation rates cannot be reasonably fit with the same intrinsic on-rate constant (kon). Perhaps the two have different diffusion coefficients, but that is unlikely given their sequence and structural similarities. In our model, the range of kons that can be used to capture elongation rates depends on the apparent kon of the data. The kon defines the rate at which incoming subunits bind the end of a protofilament (productively or transiently), while the apparent kon reflects the rate at which subunits *productively* bind the MT end (a small fraction of all binding events). Because of this, the kon can never be smaller than the apparent kon divided by 13 (the number of protofilaments), and can never be greater than the apparent kon. These two extremes correspond to two extreme modes of growth: for 1) the smallest possible kon, every addition of an incoming αβ-tubulin subunit to the MT end has to be productive; and for 2) the largest possible kon, the MT has to grow from addition to one site only, like a helix. The ranges of possible kons for our yeast and porcine data collected at 30 °C do not overlap significantly, and where they do, the longitudinal affinities needed to capture the yeast data are unreasonably high (so high that a considerable fraction of free αβ-tubulin would be dimeric at concentrations where we detect little to no dimer by AUC or gel

filtration). The upper limit of the range of kons that can capture our 30 °C porcine data (or any set of data) could be extended if we somehow incorporated conformation into our model, such that the growing MT end was partly curved. Because the MT end in our model is straight, there is always at least one empty corner site (one longitudinal + one lateral), and addition to corners is almost always productive. It is because of this that the kon can never be higher than the apparent kon in our model; but if there was on average less than one corner site (through conformational fluctuations at the MT end) a kon higher than the apparent kon could capture the data. Then we might be able to capture both yeast and porcine MT elongation rates with the same kon and reasonable affinities.

Our measurements of yeast MT dynamics are the first across a range of αβ-tubulin concentrations and at different temperatures. The differences they reveal between yeast and porcine MT dynamics shed light on the diversity of MT dynamics possible, and they provide new data with which to challenge and constrain existing models. Future experiments should be devoted to measuring 1) concentration-dependent catastrophe frequencies from porcine MTs at 30 °C, and 2) the effects of temperature change on catastrophe frequencies from both yeast and porcine MTs. It would be ideal to collect full data sets (MT elongation and shrinking rates, catastrophe frequencies) for both yeast and porcine MTs at 23 °C-- among other interesting possibilities, maybe the apparent kon of yeast αβ-tubulin will show temperature-dependence from 30 to 23°C, maybe not. Finally, our attempts to make biochemical sense of our data provide insight into the molecular origins of the differences between yeast and porcine MT dynamics.

CHAPTER FOUR

Conclusions and Future Directions

Implications of trans-acting GTP for MT catastrophe

We showed using a model of MT dynamics where the exchangeable nucleotide acts in trans that a finite rate of GDP to GTP exchange at the MT end decreased the frequency of catastrophe. We then used a mutant αβ-tubulin and a modified nucleotide impaired for binding GDP to selectively increase the rate of GDP to GTP exchange at the MT end in vitro. Elongation rates from both mutant MTs and wildtype MTs assembled in the presence of the modified nucleotide were minimally different from control (wildtype + GTP), yet they underwent catastrophe much less often. Combining the mutant and modified nucleotide resulted in an even greater decrease in the catastrophe frequency, suggesting that the two act synergistically to increase the rate of terminal nucleotide exchange. Our results suggest that terminal nucleotide exchange is important to the molecular mechanisms of MT dynamics, and provide a plausible (albeit partial) biochemical explanation for why microtubules occasionally exit otherwise sustained growth to undergo catastrophe. GDP exposure eliminates favorable binding sites on the growing end, which in turn decreases the rate of elongation and leads to catastrophe by allowing GTP hydrolysis to erode the 'stalled' GTP cap. By converting some of these unfavorable binding sites back to favorable ones, GDP to GTP exchange can extend growth lifetimes by restoring normal growth rates and preventing further erosion of the

GTP cap. The impossibility of GDP exposure at the minus-end might also explain the lower catastrophe frequencies observed for minus-end MTs in vitro.

It is worth mentioning that our model neither captures the concentration-dependence of the catastrophe frequency (predicting one that is too steep) nor MT aging. Notably, no purely biochemical model does; but the 'mechanochemical' model of VanBuren et al. from 2005 has been reported to capture both (VanBuren et al., 2005; Coombes et al., 2013). However, it has only been shown to give rise to a shallow concentration-dependence across a narrow range of αβ-tubulin concentrations (6 to 8 μM vs. 7 to 16 μM measured by Walker et al.) (Coombes et al., 2013). Also, nucleotide-state is assumed to act in cis in this model, while a growing body of evidence strongly suggests that the exchangeable nucleotide acts in trans (Buey et al., 2006; Rice et al., 2008; Nawrotek et al., 2011). Thus, the development of a model that captures all known features of MT dynamics while remaining faithful to our current knowledge is a work in progress.

Concerning the mechanism of action of our reagents, in principle, a GTPase defect might explain why mutant MTs and those assembled in the presence of modified nucleotide undergo catastrophe less often than control; but at the very least we know that our reagents are not grossly impaired for GTP hydrolysis, otherwise we would not observe catastrophe and rapid shrinking. Nevertheless, measurements of the rate of GTP hydrolysis from both mutant and wildtype MTs would be ideal; Xuecheng Ye in our lab

is currently attempting to set up a radiolabeled nucleotide-based assay to make such measurements.

Comparing MT dynamics from divergent αβ-tubulins

My measurements of microtubule dynamics are the first at multiple concentrations (spanning a 2-fold range) to come from a divergent (non-mammalian) αβ-tubulin. Unlike porcine MTs, we find that yeast MTs 1) polymerize at substantially lower concentrations (0.06 μM critical concentration vs. 1.56 μM for porcine αβ-tubulin); 2) elongate at rates that depend more steeply on concentration (4.5-fold higher apparent kon); 3) undergo plus-end-directed growth only; and 4) shrink 5-fold faster. Yeast MT polymerization dynamics also respond differently to changes in temperature: from 30 to 37 °C, the apparent kon (the rate of productive association) of yeast αβ-tubulin does not change, while the apparent kon of porcine αβ-tubulin increases by a factor of 2. Our measurements reveal interesting differences that beg a mechanistic explanation.

On the enhanced polymerization activity of yeast αβ-tubulin

Yeast αβ-tubulin affinities for the MT end have to be much higher than those of porcine αβ-tubulin to support polymerization at a much lower critical concentration (26-fold lower); our model predicts that yeast αβ-tubulin affinities have to be ~100-fold higher to support polymerization at the concentrations and rates observed. Direct measurements of self-interaction affinities for both yeast and porcine αβ-tubulin are desirable to test this prediction.

Given its relative strength and importance to MT polymerization, the longitudinal interaction is the best candidate for affinity measurements; but because of the strong tendency of αβ-tubulin to polymerize, traditional methods for measuring binding affinities (like ITC, fluorescence anisotropy, etc.) are not readily employable. One member of our lab, Beth Geyer, has recently begun attempting to measure the longitudinal affinity of yeast αβ-tubulin by AUC. Specifically, a dimer of αβ-tubulin subunits can be resolved, and the dependence of its signal's magnitude on the total concentration of αβ-tubulin can be analyzed for a binding constant; but the resulting binding constant is not well determined. Two things limit how well the binding constant can be determined: 1) the range of concentrations over which αβ-tubulin can be kept in an unaggregated state and thus measured by AUC; and 2) the strength of the longitudinal interaction. These limitations are inversely related, and if one were somehow optimal the other would invariably be most sub-optimal. Regarding the first limitation, yeast αβ-tubulin is especially hard to bring to the concentrations needed because of its strong tendency to aggregate, while porcine αβ-tubulin, by virtue of its weaker self-interactions, can be brought to much higher concentrations; but the tendency of yeast αβ-tubulin to aggregate (and polymerize) at much lower concentrations also likely reflects a stronger longitudinal interaction-- and because detection of the dimer depends on the stability of the dimer, the stronger the longitudinal interaction, the more readily detectable the dimer. Therefore, it is not clear which species of αβ-tubulin (yeast or porcine) has the better mix of properties for measurements of the longitudinal binding affinity by AUC, but both

offer the possibility and both should be measured. Additionally, mixing mutants with complementary blocking mutations (half plus-end blocked, half minus-end blocked) might enable measurements over a greater range of yeast αβ-tubulin concentrations. Because we cannot express soluble mammalian αβ-tubulin from our yeast-based overexpression system, mutants of porcine αβ-tubulin are currently not possible.

On the differential temperature-dependence of yeast and porcine MT elongation rates

The sensitivity of the apparent kon of porcine αβ-tubulin to small changes in temperature suggests the existence of an activation barrier to polymerization. This activation barrier might result from the energetic cost of straightening weakly bound curved αβ-tubulin for incorporation into the microtubule lattice. A recent study by Zanic et al. supports this idea (Zanic et al., 2013). Additionally, all structural studies show that unpolymerized αβ-tubulin is curved, while αβ-tubulin in the MT lattice is straight-- thus αβ-tubulin has to straighten during polymerization. Nevertheless, it is possible that something else accounts for the observed temperature-dependent increase in the apparent kon of porcine αβ-tubulin. Therefore, direct visualization of conformation during MT assembly would be ideal. Perhaps an intramolecular FRET pair reporting on single subunit conformation could be made. MT dynamics could then be reconstituted and monitored by TIRF.

On plus-ends and minus-ends

Yeast MTs undergo plus-end-directed growth only; and the plus- and minus-ends of porcine MTs behave differently in vitro (different rates of elongation, different

catastrophe frequencies, etc.). Thus, the first question that needs answering is what possible differences might underlie the fact that plus- and minus-ends exhibit different dynamics? In light of our results, one obvious difference between plus- and minus-ends that could lead to dynamical differences is the possibility of GDP exposure (and GDP to GTP exchange) at the plus-end. GDP exposure at the MT plus-end frustrates MT elongation by providing low affinity binding sites for incoming subunits. Frustrated growth can lead to catastrophe by allowing GTP hydrolysis to completely eat away the stalled GTP cap. The impossibility of GDP exposure on the minus-end should therefore decrease the catastrophe frequency in minus-end growing MTs. Consistent with this prediction, Walker et al. measured lower catastrophe frequencies from minus-ends than plus-ends (Walker et al., 1988). But why do we not observe any yeast microtubules growing from their minus-ends? And why is the apparent kon of porcine αβ-tubulin lower for the minus-end than the plus-end? Biochemical and structural evidence strongly suggest that free αβ-tubulin is curved independently of nucleotide-state (Buey et al., 2006, Rice et al., 2008, Nawrotek et al., 2011), and we know that αβ-tubulin in the MT lattice is straight (Mandelkow et al., 1991; Chretien et al., 1995); thus, αβ-tubulin has to straighten at or near the MT end before incorporation into the MT lattice. We infer that αβ-tubulin straightening at the minus-end likely occurs at a slower rate than straightening at the plus-end for both yeast and porcine αβ-tubulin. Mutations stabilizing the straight conformation of yeast αβ-tubulin might therefore promote MT elongation from the minus-end. We might also be able to visualize the rate of straightening at one or both ends using FRET.

Future Directions

I believe that my graduate work has laid the foundation for exciting work to come. The DIC-based assay that I set up for monitoring MT dynamics at the level of single polymers is now being used by multiple members of the lab and for a variety of purposes. With each passing month, more mutant αβ-tubulins are being purified, biochemically characterized, and used in in vitro reconstitutions of MT dynamics.

In this last chapter, I would like to give my view of what is to come (or what might come) of my work in lab, especially with respect to our in vitro reconstitutions and our computational model of MT dynamics.

Microtubule dynamics in vitro

The lab microscope is now TIRF-ready, so for the first time we can watch MT dynamics in color; this broadens the range of possible experiments at our disposal and gives us the chance to tie up some loose ends.

Polymerization-blocked αβ-tubulin is a class of mutant αβ-tubulin made in lab with substitutions at the plus- or minus-end longitudinal interface that disrupt polymerization (Johnson et al., 2011). Shortly after plus-end-blocked αβ-tubulin was used to provide us (and the world) with the first crystal structure of unpolymerized yeast αβ-tubulin (Ayaz et al., 2012), I became interested in analyzing the dose-dependence of its effects on MT

dynamics. Knowing that it could not polymerize into microtubules, we suspected that if doped into MT dynamics reactions containing wildtype αβ-tubulin it would inhibit elongation by binding the MT end and preventing further addition of incoming subunits. Thus, we predicted that it would decrease MT elongation rates and potentially increase the frequency of catastrophe in a dose-dependent manner. Experiments performed by Laura Downes, a former summer student, and Chien-Hsiang 'Charles' Hsu, a former rotation student, showed that plus-end-blocked -blocked αβ-tubulin leaves elongation rates unaltered while increasing the frequency of catastrophe (percentage of plus-end-blocked mutant assayed up to 20% of total). Does the plus-end-blocked mutant promote catastrophe by disrupting some critical end-structure? Or does it get incorporated into the MT lattice where it creates defects that weaken the growing MT? Experiments using TIRF to record MT dynamics where wildtype αβ-tubulin was labeled one color and plus-end-blocked another would allow us to determine whether plus-end-blocked αβ-tubulin binds the end or gets incorporated into the MT lattice (or both!). Such knowledge would bring needed clarity to its mechanism of action and might generate further studies.

Another class of doping experiments ideal for TIRF involves Tub1p:Tub2p-E255A. E255A is a hydrolysis-defective mutant of αβ-tubulin. Unlike plus-end-blocked αβ-tubulin, we expect E255A to have no effect on MT elongation rates while decreasing the catastrophe frequency and, potentially, increasing the rescue frequency (the switch from shrinking to growing). The mechanism of MT rescue is a mystery, but there has been some speculation that 'islands' of unhydrolyzed GTP in the MT lattice might play a role

(Dimitrov et al., 2008; Cassimeris, 2009; Tropini et al., 2012). It is possible that the location of E255A in the MT lattice will overlap nonrandomly with MT ends undergoing rescue

TIRF might also enable direct observations of nucleotide exchange at the MT end. Microtubules could be assembled in the presence of GTPγS (a nonhydrolyzable GTP analog that supports yeast MT assembly) before being diluted with buffer containing a fluorescent GTP analog. If terminal nucleotide exchange occurs then MT ends will 'light up' from the exchange of exposed GTPγS for fluorescent nucleotide.

I would also like to directly test the idea that nucleotide-state acts in trans. To this end, we could monitor MT assembly in the presence of GTPγS and then flow in GDP-bound αβ-tubulin that has been fluorescently labeled. MTs would then be diluted into pure buffer. If at the end of this procedure many MT ends have 1 subunit to a single layer of GDP-bound αβ-tubulin then nucleotide-state acts in trans; if all MT ends are free of GDP-bound αβ-tubulin then nucleotide-state *might* act in cis. Assuming trans-acting nucleotide, complete exchange of GTPγS for GDP at the MT end would prevent GDP-bound αβ-tubulin from productively binding the MT end. To avoid this possibility, it would be ideal to flow in a high concentration of GDP-bound αβ-tubulin for as short an amount of time as possible before diluting MTs into buffer (perhaps 10 seconds or less). GTPγS could also be replaced with more strongly binding GTP to reduce the rate of

terminal nucleotide exchange. Replacing GTPγS with GTP would necessitate inclusion of some MT stabilizing agent (e.g., taxol) in the dilution buffer.

Before TIRF experiments of the kind described can be performed, fluorescent-labeling strategies for yeast αβ-tubulin need to be worked out in lab. A perfusion chamber would be ideal for experiments to detect terminal nucleotide exchange and determine whether nucleotide-state acts in trans, but the lab does not currently have one. Additionally, both mutants discussed are interesting because they could easily be incorporated into our model of MT dynamics.

The model

Our model reproduces many features of MT dynamics and is parameterized reasonably given the existing data; but it predicts a catastrophe frequency that depends too steeply on αβ-tubulin concentration and is incapable of capturing MT aging. I believe that our model can be improved by incorporating conformation. Conformation is hugely important to MT dynamics: the incompatibility of the curved conformation of αβ-tubulin (and its greater stability relative to the straight conformation in free αβ-tubulin) with the MT lattice is essential to the metastability of the growing MT; and the tendency of protofilaments to curl away from the MT body in a GTP hydrolysis-dependent manner enables the rapid shrinking and turnover that drive rearrangements of the MT cytoskeleton needed in vivo. But how should we incorporate conformation into our model? I believe that one recent study (Alushin et al., 2014) strongly hints at a simple

way to incorporate GTP hydrolysis-dependent conformation at the MT end and even suggests a way to model αβ-tubulin straightening at the MT end.

Structural consequences of GTP hydrolysis inside of the MT lattice

Alushin et al. compared the structures of microtubules polymerized in the presence of GTP and GMPCPP (a nonhydrolyzable analog of GTP) in order to determine the structural consequences of GTP hydrolysis within the microtubule lattice. They obtained EM data at the highest resolution yet for MTs by employing a latest-generation electron microscope and an experimental trick for identifying the seam. Identification of the seam enabled the alignment and averaging of previously indistinguishable α- and β-tubulin subunits. Furthermore, they made full use of their data by modeling the known crystallographic structure of polymerized αβ-tubulin into their density maps using a Rosetta-based approach in lieu of rigid-body docking. They found that GTP hydrolysis and the accompanying dissociation of the unbound gamma phosphate trigger compaction of the α-subunit and a shift of its intermediate domain. This shift puts the intermediate domain in a position that strongly mirrors its conformation in free αβ-tubulin, but in free αβ-tubulin it is also rotated-- the lack of rotation seen from the shifted intermediate domain could create (or reflect) an increase in strain in the MT lattice. This strain would essentially result from the plus-end neighbors of GDP-bound subunits 'wanting' to be curved like free αβ-tubulin, and would be relieved at the MT end. There, protofilaments could relax into a curved state by curling away from the MT body. Stretches of lateral

interaction-free protofilaments would lead to rapid shrinking through the loss of subunits and oligomers of αβ-tubulin.

Accounting for GTP hydrolysis-dependent conformational change in our model

I believe that a simple addition to our model would suffice for simulating the GTP hydrolysis-dependent formation of highly curved, lateral interaction-free protofilaments at the MT end. The added rule would work as follows: if for any given protofilament, and starting from the growing end, greater than or equal to half of the last n subunits (4, say) are GDP-bound, erase all lateral interactions along length n of that protofilament. We would start by treating each protofilament independently. We would then fit in vitro MT dynamics data by 1) finding affinities that reproduced the observed rates of MT elongation; 2) finding, for one or multiple values of n, the GDP-weakening factor that reproduced the observed shrinking rate (will be lower than values needed previously); and 3) finding, again for one or multiple values of n, the GTPase and GDP to GTP exchange rate constants that reproduced the catastrophe frequency at a single concentration of αβ-tubulin. Finally, we would determine the concentration-dependence of the catastrophe frequency.

A potential concern with the rule presented above is that it ignores the seam, and recent work suggests that the seam destabilizes growing microtubules (Katsuki et al., 2014). It might be necessary to better model the seam in the future (currently, lateral interactions at the seam are assumed to have half the affinity of non-seam lateral interactions); however,

the present goal is to make the smallest change needed to meaningfully improve our model. Incorporating GTP hydrolysis-dependent conformational change at the MT end (if by the rule I suggested or some other) will, at the very least, improve the model by decreasing the presently unrealistically large GDP-weakening factor needed to capture the very rapid rate of yeast MT shrinking. It is also possible that conformation at the shrinking end will soften the concentration-dependence of the catastrophe frequency and/or reproduce MT aging.

Implications for understanding αβ-tubulin straightening & GTP-dependent assembly

Because the more or less curved conformation of αβ-tubulin at the growing MT end is key to the mechanism of action of many regulatory proteins (and might underlie the sensitive temperature-dependence we observe for porcine MT elongation rates), a complete biochemical model of MT dynamics will have to include conformation and straightening at the growing end. But where exactly does αβ-tubulin straightening matter? And might it be nucleotide-state-dependent? Our modeling and recent study on the mechanism of a MT polymerase (Ayaz et al., 2014) suggest that productive binding to the MT lattice results from binding an empty corner site and straightening into it. Alushin et al. showed that a fully incorporated αβ-tubulin subunit undergoes a conformational change when the GTP of its minus-end neighbor is hydrolyzed (Alushin et al., 2014). Their results suggest that GTP hydrolysis generates strain in the MT lattice by making the straight conformation less favorable. It follows that a curved αβ-tubulin subunit bound at a corner site on the MT end might become straight less readily if its minus-end neighbor

is GDP-bound. It is therefore possible that nucleotide-state acts in trans not by affecting the longitudinal affinity but by affecting the curved to straight transition rate (it might affect both). This would explain GTP-dependent assembly and still permit rapid shrinking from the GTP hydrolysis-dependent curling open of the MT end and accompanying loss of αβ-tubulin oligomers. Somehow incorporating this into our model would also allow us to fit yeast and porcine data with the same intrinsic on-rate constant (the range of possible kons for fitting porcine data could be increased by preventing all additions to corner sites from being productive). It would require implementing a straightening rate ('k_{strt}') for a newly added curved subunit dependent on the nucleotide-state of its minus-end neighbor. A GDP-weakening factor might not be needed with inclusion of this parameter.

Bibliography

ALUSHIN, G. M., LANDER, G. C., KELLOGG, E. H., ZHANG, R., BAKER, D. & NOGALES, E. 2014. High-resolution microtubule structures reveal the structural transitions in alphabeta-tubulin upon GTP hydrolysis. *Cell,* 157**,** 1117-29.

AMAYED, P., CARLIER, M. F. & PANTALONI, D. 2000. Stathmin slows down guanosine diphosphate dissociation from tubulin in a phosphorylation-controlled fashion. *Biochemistry,* 39**,** 12295-302.

AYAZ, P., MUNYOKI, S., GEYER, E. A., PIEDRA, F. A., VU, E. S., BROMBERG, R., OTWINOWSKI, Z., GRISHIN, N. V., BRAUTIGAM, C. A. & RICE, L. M. 2014. A tethered delivery mechanism explains the catalytic action of a microtubule polymerase. *Elife***,** e03069.

AYAZ, P., YE, X., HUDDLESTON, P., BRAUTIGAM, C. A. & RICE, L. M. 2012. A TOG:alphabeta-tubulin complex structure reveals conformation-based mechanisms for a microtubule polymerase. *Science,* 337**,** 857-60.

AYLETT, C. H. & LOWE, J. 2012. Superstructure of the centromeric complex of TubZRC plasmid partitioning systems. *Proc Natl Acad Sci U S A,* 109**,** 16522-7.

BAYLEY, P. M., SCHILSTRA, M. J. & MARTIN, S. R. 1989. A simple formulation of microtubule dynamics: quantitative implications of the dynamic instability of microtubule populations in vivo and in vitro. *J Cell Sci,* 93 (Pt 2)**,** 241-54.

BECHSTEDT, S. & BROUHARD, G. J. 2012. Doublecortin recognizes the 13-protofilament microtubule cooperatively and tracks microtubule ends. *Dev Cell,* 23**,** 181-92.

BELMONT, L. D. & MITCHISON, T. J. 1996. Identification of a protein that interacts with tubulin dimers and increases the catastrophe rate of microtubules. *Cell,* 84**,** 623-31.

BORISY, G. G. & TAYLOR, E. W. 1967a. The mechanism of action of colchicine. Binding of colchincine-3H to cellular protein. *J Cell Biol,* 34**,** 525-33.

BORISY, G. G. & TAYLOR, E. W. 1967b. The mechanism of action of colchicine. Colchicine binding to sea urchin eggs and the mitotic apparatus. *J Cell Biol,* 34**,** 535-48.

BOWNE-ANDERSON, H., ZANIC, M., KAUER, M. & HOWARD, J. 2013. Microtubule dynamic instability: a new model with coupled GTP hydrolysis and multistep catastrophe. *Bioessays,* 35**,** 452-61.

BROUHARD, G. J. & RICE, L. M. 2014. The contribution of alphabeta-tubulin curvature to microtubule dynamics. *J Cell Biol,* 207**,** 323-34.

BRUN, L., RUPP, B., WARD, J. J. & NEDELEC, F. 2009. A theory of microtubule catastrophes and their regulation. *Proc Natl Acad Sci U S A,* 106**,** 21173-8.

BUEY, R. M., DIAZ, J. F. & ANDREU, J. M. 2006. The nucleotide switch of tubulin and microtubule assembly: a polymerization-driven structural change. *Biochemistry,* 45**,** 5933-8.

BURNS, R. G. 1991. Alpha-, beta-, and gamma-tubulins: sequence comparisons and structural constraints. *Cell Motil Cytoskeleton,* 20**,** 181-9.

BURRIS, J. E. & SEGAL, S. 1994. A Tribute to Professor Dan,Katsuma on His 90th Birthday. *Biological Bulletin,* 187**,** 125-130.

CAPLOW, M. & SHANKS, J. 1995. Induction of microtubule catastrophe by formation of tubulin-GDP and apotubulin subunits at microtubule ends. *Biochemistry,* 34**,** 15732-41.

CARLIER, M. F. 1982. Guanosine-5'-triphosphate hydrolysis and tubulin polymerization. Review article. *Mol Cell Biochem,* 47**,** 97-113.

CARLIER, M. F., HILL, T. L. & CHEN, Y. 1984. Interference of GTP hydrolysis in the mechanism of microtubule assembly: an experimental study. *Proc Natl Acad Sci U S A,* 81**,** 771-5.

CARLIER, M. F. & PANTALONI, D. 1978. Kinetic analysis of cooperativity in tubulin polymerization in the presence of guanosine di- or triphosphate nucleotides. *Biochemistry,* 17**,** 1908-15.

CARLIER, M. F. & PANTALONI, D. 1981. Kinetic analysis of guanosine 5'-triphosphate hydrolysis associated with tubulin polymerization. *Biochemistry,* 20**,** 1918-24.

CASSIMERIS, L. 2009. Microtubule assembly: lattice GTP to the rescue. *Curr Biol,* 19**,** R174-6.

CHEN, Y. & HILL, T. L. 1983. Use of Monte Carlo calculations in the study of microtubule subunit kinetics. *Proc Natl Acad Sci U S A,* 80**,** 7520-3.

CHEN, Y. D. & HILL, T. L. 1985. Monte Carlo study of the GTP cap in a five-start helix model of a microtubule. *Proc Natl Acad Sci U S A,* 82**,** 1131-5.

CHOI, M. C., RAVIV, U., MILLER, H. P., GAYLORD, M. R., KIRIS, E., VENTIMIGLIA, D., NEEDLEMAN, D. J., KIM, M. W., WILSON, L., FEINSTEIN, S. C. & SAFINYA, C. R. 2009. Human microtubule-associated-protein tau regulates the number of protofilaments in microtubules: a synchrotron x-ray scattering study. *Biophys J,* 97**,** 519-27.

CHRETIEN, D., FULLER, S. D. & KARSENTI, E. 1995. Structure of growing microtubule ends: two-dimensional sheets close into tubes at variable rates. *J Cell Biol,* 129**,** 1311-28.

CONDE, C. & CACERES, A. 2009. Microtubule assembly, organization and dynamics in axons and dendrites. *Nat Rev Neurosci,* 10**,** 319-32.

COOMBES, C. E., YAMAMOTO, A., KENZIE, M. R., ODDE, D. J. & GARDNER, M. K. 2013. Evolving tip structures can explain age-dependent microtubule catastrophe. *Curr Biol,* 23**,** 1342-8.

DAVIS, A., SAGE, C. R., WILSON, L. & FARRELL, K. W. 1993. Purification and biochemical characterization of tubulin from the budding yeast Saccharomyces cerevisiae. *Biochemistry,* 32**,** 8823-35.

DELL, K. R. & VALE, R. D. 2004. A tribute to Shinya Inoue and innovation in light microscopy. *J Cell Biol,* 165**,** 21-5.

DESAI, A. & MITCHISON, T. J. 1997. Microtubule polymerization dynamics. *Annu Rev Cell Dev Biol,* 13**,** 83-117.

DETRICH, H. W., 3RD, PARKER, S. K., WILLIAMS, R. C., JR., NOGALES, E. & DOWNING, K. H. 2000. Cold adaptation of microtubule assembly and dynamics. Structural interpretation of primary sequence changes present in the alpha- and beta-tubulins of Antarctic fishes. *J Biol Chem,* 275**,** 37038-47.

DIMITROV, A., QUESNOIT, M., MOUTEL, S., CANTALOUBE, I., POUS, C. & PEREZ, F. 2008. Detection of GTP-tubulin conformation in vivo reveals a role for GTP remnants in microtubule rescues. *Science,* 322**,** 1353-6.

ETTEMA, T. J., LINDAS, A. C. & BERNANDER, R. 2011. An actin-based cytoskeleton in archaea. *Mol Microbiol,* 80**,** 1052-61.

EDELSTEIN, A., AMODAJ, N., HOOVER, K., VALE, R. & STUURMAN, N. 2010. Computer control of microscopes using microManager. *Curr Protoc Mol Biol,* Chapter 14**,** Unit14 20.

ERICKSON, H. P. & PANTALONI, D. 1981. The role of subunit entropy in cooperative assembly. Nucleation of microtubules and other two-dimensional polymers. *Biophys J,* 34**,** 293-309.

FISHBACK, J. L. & YARBROUGH, L. R. 1984. Interaction of 6-mercapto-GTP with bovine brain tubulin. Equilibrium aspects. *J Biol Chem,* 259**,** 1968-73.

FLEMMING, W. 1965. Historical Paper. Contributions to the Knowledge of the Cell and Its Vital Processes. *J Cell Biol,* 25**,** SUPPL:1-69.

FYGENSON, D. K., BRAUN, E. & LIBCHABER, A. 1994. Phase diagram of microtubules. *Phys Rev E Stat Phys Plasmas Fluids Relat Interdiscip Topics,* 50**,** 1579-1588.

GARDEL ML, V. M., WEITZ DA. 2005. Microrheology. *In:* K, B. (ed.) *Microscale Diagnostic Techniques.* Springer Verlag.

GARDNER, M. K., CHARLEBOIS, B. D., JANOSI, I. M., HOWARD, J., HUNT, A. J. & ODDE, D. J. 2011a. Rapid microtubule self-assembly kinetics. *Cell,* 146**,** 582-92.

GARDNER, M. K., ZANIC, M., GELL, C., BORMUTH, V. & HOWARD, J. 2011b. Depolymerizing kinesins Kip3 and MCAK shape cellular microtubule architecture by differential control of catastrophe. *Cell,* 147**,** 1092-103.

GARNER, E. C., CAMPBELL, C. S., WEIBEL, D. B. & MULLINS, R. D. 2007. Reconstitution of DNA segregation driven by assembly of a prokaryotic actin homolog. *Science,* 315**,** 1270-4.

GELL, C., BORMUTH, V., BROUHARD, G. J., COHEN, D. N., DIEZ, S., FRIEL, C. T., HELENIUS, J., NITZSCHE, B., PETZOLD, H., RIBBE, J., SCHAFFER, E., STEAR, J. H., TRUSHKO, A., VARGA, V., WIDLUND, P. O., ZANIC, M. & HOWARD, J. 2010. Microtubule dynamics reconstituted in vitro and imaged by single-molecule fluorescence microscopy. *Methods Cell Biol,* 95**,** 221-45.

GIGANT, B., CURMI, P. A., MARTIN-BARBEY, C., CHARBAUT, E., LACHKAR, S., LEBEAU, L., SIAVOSHIAN, S., SOBEL, A. & KNOSSOW, M. 2000. The 4 A X-ray structure of a tubulin:stathmin-like domain complex. *Cell,* 102**,** 809-16.

GOODSON, H. V. & GREGORETTI, I. V. 2010. Using Computational Modeling to Understand Microtubule Dynamics: A Primer for Cell Biologists. *Microtubules, in Vitro,* 95**,** 175-188.

GRAUMANN, P. L. 2007. Cytoskeletal elements in bacteria. *Annu Rev Microbiol,* 61**,** 589-618.

GUPTA, M. L., JR., BODE, C. J., THROWER, D. A., PEARSON, C. G., SUPRENANT, K. A., BLOOM, K. S. & HIMES, R. H. 2002. beta-Tubulin C354 mutations that severely decrease microtubule dynamics do not prevent nuclear migration in yeast. *Mol Biol Cell,* 13**,** 2919-32.

HILL, T. L. & KIRSCHNER, M. W. 1982. Bioenergetics and kinetics of microtubule and actin filament assembly-disassembly. *Int Rev Cytol,* 78**,** 1-125.

HONNAPPA, S., CUTTING, B., JAHNKE, W., SEELIG, J. & STEINMETZ, M. O. 2003. Thermodynamics of the Op18/stathmin-tubulin interaction. *J Biol Chem,* 278**,** 38926-34.

HORIO, T. & HOTANI, H. 1986. Visualization of the dynamic instability of individual microtubules by dark-field microscopy. *Nature,* 321**,** 605-7.

HOWARD, J. & HYMAN, A. A. 2003. Dynamics and mechanics of the microtubule plus end. *Nature,* 422**,** 753-8.

HYMAN, A. A., CHRETIEN, D., ARNAL, I. & WADE, R. H. 1995. Structural changes accompanying GTP hydrolysis in microtubules: information from a slowly hydrolyzable analogue guanylyl-(alpha,beta)-methylene-diphosphonate. *J Cell Biol,* 128**,** 117-25.

INOUE, S. 1951. *Studies of the structure of the mitotic spindle in living cells with an improved polarization microscope.* Ph.D, Princeton University.

INOUE, S. 1953. [Polarization optical studies of the mitotic spindle. I. The demonstration of spindle fibers in living cells]. *Chromosoma,* 5**,** 487-500.

INOUE, S. 1959. Motility of Cilia and the Mechanism of Mitosis. *Reviews of Modern Physics,* 31**,** 402-408.

INOUE, S. 1981. Cell division and the mitotic spindle. *J Cell Biol,* 91**,** 131s-147s.

INOUE, S. 2008. Microtubule dynamics in cell division: exploring living cells with polarized light microscopy. *Annu Rev Cell Dev Biol,* 24**,** 1-28.

INOUE, S. & SALMON, E. D. 1995. Force generation by microtubule assembly/disassembly in mitosis and related movements. *Mol Biol Cell,* 6**,** 1619-40.

JOHNSON, V., AYAZ, P., HUDDLESTON, P. & RICE, L. M. 2011. Design, overexpression, and purification of polymerization-blocked yeast alphabeta-tubulin mutants. *Biochemistry,* 50**,** 8636-44.

KATSUKI, M., DRUMMOND, D. R. & CROSS, R. A. 2014. Ectopic A-lattice seams destabilize microtubules. *Nat Commun,* 5**,** 3094.

KOREN, R. & HAMMES, G. G. 1976. A kinetic study of protein-protein interactions. *Biochemistry,* 15**,** 1165-71.

KOSHLAND, D. *Protocol: cycling tubulin (from the lab of Doug Koshland)* [Online]. Available: http://mcb.berkeley.edu/labs/koshland/Protocols/MICROTUBULE/cyclingmicrotub.html [Accessed].

KRAEMER, J. A., ERB, M. L., WADDLING, C. A., MONTABANA, E. A., ZEHR, E. A., WANG, H., NGUYEN, K., PHAM, D. S., AGARD, D. A. & POGLIANO, J. 2012. A phage tubulin assembles dynamic filaments by an atypical mechanism to center viral DNA within the host cell. *Cell,* 149**,** 1488-99.

MANDELKOW, E. M., MANDELKOW, E. & MILLIGAN, R. A. 1991. Microtubule dynamics and microtubule caps: a time-resolved cryo-electron microscopy study. *J Cell Biol,* 114**,** 977-91.

MARGOLIN, G., GREGORETTI, I. V., CICKOVSKI, T. M., LI, C., SHI, W., ALBER, M. S. & GOODSON, H. V. 2012. The mechanisms of microtubule catastrophe and rescue: implications from analysis of a dimer-scale computational model. *Mol Biol Cell,* 23**,** 642-56.

MELKI, R., CARLIER, M. F., PANTALONI, D. & TIMASHEFF, S. N. 1989. Cold depolymerization of microtubules to double rings: geometric stabilization of assemblies. *Biochemistry,* 28**,** 9143-52.

MITCHISON, T. & KIRSCHNER, M. 1984a. Dynamic instability of microtubule growth. *Nature,* 312**,** 237-42.

MITCHISON, T. & KIRSCHNER, M. 1984b. Microtubule assembly nucleated by isolated centrosomes. *Nature,* 312**,** 232-7.

MITCHISON, T. J. 1993. Localization of an exchangeable GTP binding site at the plus end of microtubules. *Science,* 261**,** 1044-7.

MITCHISON, T. J. 2013. A question of taste. *Mol Biol Cell,* 24**,** 3278-80.

MOHRI, H. 1968. Amino-acid composition of "Tubulin" constituting microtubules of sperm flagella. *Nature,* 217**,** 1053-4.

MOLECULAR PROBES, I. SYPRO® Ruby Protein Gel Stain. Available: https://tools.lifetechnologies.com/content/sfs/manuals/mp12000.pdf.

NAWROTEK, A., KNOSSOW, M. & GIGANT, B. 2011. The determinants that govern microtubule assembly from the atomic structure of GTP-tubulin. *J Mol Biol,* 412**,** 35-42.

NEFF, N. F., THOMAS, J. H., GRISAFI, P. & BOTSTEIN, D. 1983. Isolation of the beta-tubulin gene from yeast and demonstration of its essential function in vivo. *Cell,* 33**,** 211-9.

NOGALES, E., DOWNING, K. H., AMOS, L. A. & LOWE, J. 1998a. Tubulin and FtsZ form a distinct family of GTPases. *Nat Struct Biol,* 5**,** 451-8.

NOGALES, E. & WANG, H. W. 2006. Structural mechanisms underlying nucleotide-dependent self-assembly of tubulin and its relatives. *Curr Opin Struct Biol,* 16**,** 221-9.

NOGALES, E., WOLF, S. G. & DOWNING, K. H. 1998b. Structure of the alpha beta tubulin dimer by electron crystallography. *Nature,* 391**,** 199-203.

NORTHRUP, S. H. & ERICKSON, H. P. 1992. Kinetics of protein-protein association explained by Brownian dynamics computer simulation. *Proc Natl Acad Sci U S A,* 89**,** 3338-42.

OKADA, M. 1996. Katsuma Dan - Obituary. *Development Growth & Differentiation,* 38**,** 449-449.

OLIVA, M. A., MARTIN-GALIANO, A. J., SAKAGUCHI, Y. & ANDREU, J. M. 2012. Tubulin homolog TubZ in a phage-encoded partition system. *Proc Natl Acad Sci U S A,* 109**,** 7711-6.

PAWELETZ, N. 2001. Walther Flemming: pioneer of mitosis research. *Nat Rev Mol Cell Biol,* 2**,** 72-5.

PECQUEUR, L., DUELLBERG, C., DREIER, B., JIANG, Q., WANG, C., PLUCKTHUN, A., SURREY, T., GIGANT, B. & KNOSSOW, M. 2012. A designed ankyrin repeat protein selected to bind to tubulin caps the microtubule plus end. *Proc Natl Acad Sci U S A,* 109**,** 12011-6.

POLKA, J. K., KOLLMAN, J. M., AGARD, D. A. & MULLINS, R. D. 2009. The structure and assembly dynamics of plasmid actin AlfA imply a novel mechanism of DNA segregation. *J Bacteriol,* 191**,** 6219-30.

PUCCIARELLI, S., BALLARINI, P., SPARVOLI, D., BARCHETTA, S., YU, T., DETRICH, H. W., 3RD & MICELI, C. 2012. Distinct functional roles of beta-tubulin isotypes in microtubule arrays of Tetrahymena thermophila, a model single-celled organism. *PLoS One,* 7**,** e39694.

RAFF, E. C., FACKENTHAL, J. D., HUTCHENS, J. A., HOYLE, H. D. & TURNER, F. R. 1997. Microtubule architecture specified by a beta-tubulin isoform. *Science,* 275**,** 70-3.

RAVELLI, R. B., GIGANT, B., CURMI, P. A., JOURDAIN, I., LACHKAR, S., SOBEL, A. & KNOSSOW, M. 2004. Insight into tubulin regulation from a complex with colchicine and a stathmin-like domain. *Nature,* 428**,** 198-202.

REDEKER, V., LECAER, J. P. & ROSSIER, J. 1993. Posttranslational Glutamylation of Several Brain Tubulin Isotypes - Structure of the Polyglutamyl Side-Chain. *Methods in Protein Sequence Analysis***,** 183-190.

RICE, L. M., MONTABANA, E. A. & AGARD, D. A. 2008. The lattice as allosteric effector: structural studies of alphabeta- and gamma-tubulin clarify the role of GTP in microtubule assembly. *Proc Natl Acad Sci U S A,* 105**,** 5378-83.

SCHATZ, P. J., PILLUS, L., GRISAFI, P., SOLOMON, F. & BOTSTEIN, D. 1986. Two functional alpha-tubulin genes of the yeast Saccharomyces cerevisiae encode divergent proteins. *Mol Cell Biol,* 6**,** 3711-21.

SCHNEIDER, C. A., RASBAND, W. S. & ELICEIRI, K. W. 2012. NIH Image to ImageJ: 25 years of image analysis. *Nat Methods,* 9**,** 671-5.

SCHWARZ, P. M., LIGGINS, J. R. & LUDUENA, R. F. 1998. Beta-tubulin isotypes purified from bovine brain have different relative stabilities. *Biochemistry,* 37**,** 4687-92.

SHIH, Y. L. & ROTHFIELD, L. 2006. The bacterial cytoskeleton. *Microbiol Mol Biol Rev,* 70**,** 729-54.

SIRAJUDDIN, M., RICE, L. M. & VALE, R. D. 2014. Regulation of microtubule motors by tubulin isotypes and post-translational modifications. *Nat Cell Biol,* 16**,** 335-44.

TROPINI, C., ROTH, E. A., ZANIC, M., GARDNER, M. K. & HOWARD, J. 2012. Islands containing slowly hydrolyzable GTP analogs promote microtubule rescues. *PLoS One,* 7**,** e30103.

VANBUREN, V., CASSIMERIS, L. & ODDE, D. J. 2005. Mechanochemical model of microtubule structure and self-assembly kinetics. *Biophys J,* 89**,** 2911-26.

VANBUREN, V., ODDE, D. J. & CASSIMERIS, L. 2002. Estimates of lateral and longitudinal bond energies within the microtubule lattice. *Proc Natl Acad Sci U S A,* 99**,** 6035-40.

WALKER, R. A., O'BRIEN, E. T., PRYER, N. K., SOBOEIRO, M. F., VOTER, W. A., ERICKSON, H. P. & SALMON, E. D. 1988. Dynamic instability of individual microtubules analyzed by video light microscopy: rate constants and transition frequencies. *J Cell Biol,* 107**,** 1437-48.

WANG, H. W. & NOGALES, E. 2005. Nucleotide-dependent bending flexibility of tubulin regulates microtubule assembly. *Nature,* 435**,** 911-5.

WATERMAN-STORER, C. M. 2001. Microtubule/organelle motility assays. *Curr Protoc Cell Biol,* Chapter 13**,** Unit 13 1.

WEISENBERG, R. C. 1972. Microtubule formation in vitro in solutions containing low calcium concentrations. *Science,* 177**,** 1104-5.

WELLS, W. A. 2005a. The discovery of tubulin. *J Cell Biol.,* 169**,** 1.

WELLS, W. A. 2005b. Microtubules get a name. *J Cell Biol.,* 168**,** 2.

WICKSTEAD, B. & GULL, K. 2011. The evolution of the cytoskeleton. *J Cell Biol,* 194**,** 513-25.

YARBROUGH, L. R. & FISHBACK, J. L. 1985. Kinetics of interaction of 2-amino-6-mercapto-9-beta-ribofuranosylpurine 5'-triphosphate with bovine brain tubulin. *Biochemistry,* 24**,** 1708-14.

ZANIC, M., WIDLUND, P. O., HYMAN, A. A. & HOWARD, J. 2013. Synergy between XMAP215 and EB1 increases microtubule growth rates to physiological levels. *Nat Cell Biol,* 15**,** 688-93.